Aus dem Institut für Klinische Radiologie

der

Ludwig-Maximillians-Universität München

Direktor : Prof. Dr. med. Dr. h.c. M. Reiser

Superparamagnetic Iron Oxide (SPIO)-enhanced Liver MR Imaging with

Ferucarbotran: Efficacy for Characterization of Focal Liver Lesions with T2-

weighted FSE and T2*-weighted GRE and Early Dynamic T1-weighted GRE

sequences

Dissertation

zum Erwerb des Doktorgrades der Medizin

an der Medizinischen Fakultät der

Ludwig-Maximillians-Universität zu München

vorgelegt von

Sook Namkung

aus

Chuncheon, Süd-Korea

2006

Mit Genehmigung der Medizinischen Fakultät
der Universität München

Berichterstatter :   PD Dr. med. S. Schönberg

Mitberichterstatter :   Priv. Doz. Dr. R. Tilling

                                            Prof. Dr. A. Gerbes

Mitbetreuung durch den

Promovierten Mitarbeiter :   Dr. med. C. Zech

Dekan :   Prof. Dr. med. D. Reinhardt

Tag der mündlichen Prüfung :   19.10.2006

Index of Contents

Index of Abbreviations

CCC	CholangioCellular Carcinoma
CE	Contrast-Enhanced
CNR	Contrast-to-Noise Ratio
CT	Computed Tomography
CTAP	Computed Tomography during Arterial Portography
FNH	Focal Nodular Hyperplasia
FSE	Fast-Spin Echo
GI	GastroIntestinal
GRE	GRadient Echo
HCC	HepatoCellular Carcinoma
i.e.	id est (that is)
IVC	Inferior Vena Cava
MION	Monocrystalline Iron Oxide Nanoparticle
MR	Magnetic Resonance
MRA	Magnetic Resonance Angiography
MRI	Magnetic Resonance Imaging
N	not identified
NA	not applicable
NCE	Non-Contrast-Enhanced
NS	not significant
n.s.	not significant
1.5-T	1.5-Tesla
PACS	Picture Archiving and Communicating System
p.o.	per oral
PSIL	Percentage of Signal Intensity Loss
RES	ReticuloEndothelial System
ROI	Region-Of-Interest
SE	Spin Echo
SI	Signal Intensity
SNR	Signal-to-Noise Ratio
SPIO	SuperParamagnetic Iron Oxide
SSPIO	Standard SuperParamagnetic Iron Oxide
3D-GRE VIBE	3-Dimentional Volumetric Interpolated Breath-hold
2D-GRE	Examination

T1-w /T2-w/T2*-w	2-Dimentional Gradient Echo
TACE	T1-weighted/T2-weighted/T2*-weighted
TE	Transcatheter Arterial ChemoEmbolization
TR	Echo Time
USPIO	Repetition Time
	Ultrasmall SuperParamagnetic Iron Oxide

1. INTRODUCTION

An early and accurate diagnosis and differentiation from potentially benign focal liver lesions is important for the appropriate and successful treatment of patients with malignant liver tumors, because it influences the decisions on the therapeutic options such as surgical resection, liver transplantation, transcatheter arterial chemoembolization (TACE), percutaneous ethanol or radiofrequency ablation (8,52,57).

In selected patients with hepatocellular carcinoma (HCC) or liver metastases, improved survival can be achieved with surgical resection, and preoperative evaluation of the number, size, and segmental location of lesions is very important (22,45). Computed tomography during arterial portography (CTAP) is considered the most sensitive preoperative imaging modality for the detection of liver lesions, with reported sensitivities of 81%-93% (21,26,29,50). However, it has potential disadvantages such as invasiveness of the procedure and the high rate of false-positive findings due to the difficulties to differentiate benign liver lesions (such as adenoma, hemangioma or focal nodular hyperplasia), non-tumorous portal vein perfusion defects and small cysts from malignant lesions (7,38).

Magnetic resonance imaging (MRI) after bolus injection of extracellular paramagnetic gadolinium chelates is a useful and non-invasive technique for the characterization of focal liver lesions to study tumor enhancement pattern at dynamic T1-weighted (w) MRI. However, although characterization of focal liver lesions is possible in gadolinium-enhanced MRI with sensitivities between 75.3 to 100%, CTAP is considered to be superior for tumor detection (15,18, 20,37,47,59).

Liver-specific contrast agents, such as superparamagnetic iron oxide (SPIO) particles, have been developed to increase the potential of MR imaging for the detection and characterization of focal liver lesions (2,3). SPIO particles are taken up by the reticulo-endothelial system (RES) cells, so called Kupffer cells, of normal liver parenchyma as well as by macrophages of the spleen and lymph nodes and shorten T2 and T2* relaxation time by disturbing the local magnetic field in the liver parenchyma, thereby resulting in a signal intensity (SI) loss of normal liver parenchyma (16,25,40,54).

Malignant liver tumors do not have a substantial number of RES cells and appear as hyperintense lesions contrasting versus the hypointense liver parenchyma after application of SPIO on T2-w MR imaging. Thereby the detection of focal liver lesions can be improved due to the increased tumor-to-liver tissue contrast (1,11,28,36,43). In addition, SPIO particles can also be used for the characterization of focal liver lesions based on tumor cell composition and function (2,3)

In several articles the reported sensitivities for the detection of focal liver lesions was equivalent for SPIO-enhanced MRI and CTAP with the specificity being substantially higher for SPIO-enhanced MRI. Therefore, SPIO-enhanced MRI is considered a useful method with a high preoperative diagnostic efficacy (4,10,28,46,48).

In earlier clinical trials the effects of SPIO particles were evaluated almost exclusively on T2-w fast spin echo (FSE) and T2*-w gradient echo (GRE) sequences, whereas usually not much attention was paid to T1-w GRE sequences (1,24, 40,51,54,58). However, the effect of SPIO particles on proton relaxation is not confined to T2 and T2*. They also influence T1 relaxivity with increased SI on T1-w GRE sequences at low concentrations (9,49).

The newly developed SPIO ferucarbotran (Resovist^{TM}, Schering, Germany) has shown

promising results in terms of safety as well as in terms of detection and characterization of focal liver lesions (4,6,40,54). In contrast to other SPIO agents it can be injected rapidly as an intravenous bolus and has demonstrated T1 shortening effects in the early perfusion phase following rapid bolus injection. Therefore, with ferucarbotran dynamic imaging can be performed, although the amount and pattern of enhancement in liver vessels and focal liver lesions is not considered equivalent to gadolinium chelates (34,39, 41,54).

The purposes of our study are

- first, we wanted to evaluate and compare the efficacy of ferucarbotran-enhanced T2-w FSE and T2*-w GRE sequences at 1.5 T for the characterization of focal liver lesions and to find out characteristic findings of each benign and malignant lesions by means of quantitative and qualitative analyses.

- second, we hypothesized that ferucarbotran-enhanced dynamic T1-w GRE MRI may contribute to improved characterization of focal liver lesions and that specific enhancement patterns for different focal liver lesions might exist; we, therefore, evaluated the enhancement of liver parenchyma, liver vasculature and different focal liver lesions after bolus injection of ferucarbotran in early dynamic MRI with T1-w 2D-GRE and 3D-GRE sequences.

1.1 Classification of SPIO Agents (56)

SPIO contrast agents include oral (large) SPIO agents, standard SPIO (SSPIO) agents,

ultrasmall SPIO (USPIO) agents and monocrystalline iron oxide nanoparticle (MION) agents. The former three kinds of agents have been approved for clinical application or are being clinically tested, under various generic names and trade names (Table 1,2). MION agents are still at the experimental study stage.

Agent	Classification	Generic name	Trade name	Developing company
AMI-121	Oral SPIO	Ferumoxsil	Lumirem	Guerbet
			Gastromark	Advanced Magnetics
OMP	Oral SPIO		Abdoscan	Nycomed
AMI-25	SSPIO	Ferumoxide	Endorem	Guerbet
			Feridex IV	Berlex Laboratories
SHU 555A	SSPIO	Ferucarbotran	Resovist	Schering
AMI-227	USPIO	Ferumoxtran	Sinerem	Guerbet
			Combidex	Advanced Magnetics
NC100150	USPIO		Clariscan	Nycomed

Table 1: The generic and (planned) trade names of superparamagnetic iron oxide (SPIO) agents which are approved or in clinical development.

Agent	Particle size	Target organs	Dose	Mode of administration
AMI-121	300 nm	GI lumen	1.5-3.9 mmol^{-1} l Fe 400-600 ml	p.o.
OMP	3.5 μm	GI lumen	0.5 g/l 400-600 ml	p.o.
AMI-25	80-150 nm	Liver/spleen	15 μmol Fe/kg	Slow infusion
SHU 555A	62 nm	Liver/spleen	8 μmol Fe/kg	Bolus infusion
		Perfusion	4-16 μmol Fe/kg	Bolus infusion
		MRA	10 μmol Fe/kg	Bolus infusion
AMI-227	20-40 nm	Lymph nodes	30-45 μmol Fe/kg	Slow infusion
		MRA	14-30 μmol Fe/kg	Slow infusion
NC100150	20 nm	Perfusion	7 μmol Fe/kg	Bolus infusion
		MRA	50-100 μmol Fe/kg	Bolus infusion

Table 2 : Properties and applications of superparamagnetic iron oxide (SPIO) agents
Note- GI; Gastrointestinal,   MRA; MR Angiography,   p.o.; per oral

1.1.1 SSPIO Agents for Liver MR Imaging (16,17,33,41,56)

Ferumoxide (AMI-25, Endorem™ by Guerbet and Feridex™ by Berlex Laboratories) is coated with dextran, the iron oxide crystal is 4.8-5.6 nm, and the hydrodynamic diameter is 80-150 nm. The T2 and T1 relaxivities are 98.3 and 23.9 mmol^{-1} l s^{-1} respectively. Ferumoxide efficiently accumulates in the liver (approximately 80% of the injected dose) and spleen (5-10% of injected dose) within minutes of administration; blood half-life is 6 min. Peak concentration of iron were found in liver after 2 hours and in the spleen after 4 hours. Iron is slowly cleared from liver (half-life, 3 days) and spleen (half-life: 4 days). Ferumoxide is usually not bolus-injected because of cardiovascular side effects and severe lumbar pain. About 3.6% of all subjects experienced some type of lower back pain or leg pain during the infusion. The occurrence of these events was higher in cirrhotic patients. However, in most patients, these adverse reactions subsided following a short interruption in the infusion. The recommended mode of administration is a dose of 15 μmol Fe/kg in 100 ml of glucose 5% and a biphasic infusion (2 ml/min over 10 min and 4 ml/min over 20 min). Ferumoxide allows a wide scan window for T2/T2* weighted imaging (0.5~6 hours after administration).

Ferucarbotran (SHU 555A, Resovist™, Schering, Germany) is a SSPIO characterized by a carboxydextran rather than dextran coating. The crystal of ferucarbotran is 4.2 nm and the hydrodynamic diameter is 62 nm. The carboxydextran coating (27-35 mg/ml with an iron-to-carboxydextran ratio of 1:1 [weight-to-weight ratio]) ensures aqueous solubility of the microparticles and prevents aggregation. Ferucarbotran is an aqueous

suspension containing 0.5 mol/l of iron, 40 mg/ml mannitol and 2 mg/ml of lactatic acid, which is adjusted to a pH of 6.5 at 37 degree Celsius. The solution has an osmolarity of 0.319 osmol/kg H_2O and a viscosity of 1,031 Mpa·sec at 37 degree Celsius. The T1 relaxivity is 25.4 mmol/l^{-1} s^{-1} and T2 relaxivy is 151.0 mmol/l^{-1} s^{-1}. Unlike ferumoxide, ferucarbotran does not show side effects after rapid intravenous injection. A dose of 8 µmol Fe/kg is the recommended quantity for liver T2-w imaging at retention phase (after the SPIO particles have been trapped by the phagocytes), which can be scanned 30 min after administration. Due to its smaller size and thus stronger T1 relaxation property, ferucarbotran has also been used for T1-w imaging and MR angiography. Dynamic T1-w MR imaging following bolus infusion of ferucarbotran mimics signal changes caused by gadolinium chelates.

1.2 Review of Gadolinium Chelates-enhanced Liver MR Imaging (2,3,23)

Dynamic imaging after bolus injection of a gadolinium chelates may currently be the single most important component of an MR examination of the abdomen in numerous circumstances, particularly for the detection and characterization of liver lesions. Images are obtained during four phases relative to the injection of the contrast agent: precontrast; arterial (pre-sinusoidal); portal venous (sinusoidal); delayed (extracellular) phase.

There are two physiologic principles that allow targeting contrast enhancement: the dual blood supply of the liver and the hemodynamics of hepatic tumors. The liver is unique among abdominal organs in having a dual blood supply, with the portal vein supplying

75% to 80% of flow and the hepatic arterial supplying the remaining 20% to 25%. Liver tumors, however, receive nearly all their blood supply from the hepatic artery. Hepatic tumors are divided into hypovascular or hypervascular, relative to the vascularity of the liver. Most benign and malignant hepatic masses are relatively hypovascular, and are best detected as low SI lesions against a background of a maximally enhanced liver achieved during the portal venous dominant phase of hepatic enhancement. Tumors that are considered hypervascular receive a rich hepatic arterial flow and enhance to a similar degree as liver parenchyma, and may not be detected on the portal venous dominant phase of enhancement. They are best detected on the arterial dominant phase of enhancement.

1.2.1 Extracellular Contrast Agents

A variety of different gadolinium chelate formulations are used as extracellular contrast agents, these are nonspecific substances, enhancing the extracellular fluid spaces. These contrast agents are considered essential for standard MR imaging examination of the liver, especially in imaging of HCC or hypervascular malignant tumors. After intravenous bolus administration, gadolinium is distributed rapidly from the vascular compartment into the extracellular space prior to renal excretion. The usual clinical dose of gadolinium chelates is 0.1 mmol/kg body weight. Gadolinium has paramagnetic complexes that reduce T1 relaxivity to a much greater extent than T2 relaxivity, resulting in tissue signal intensity increases on T1-w images. In general, maximum contrast effect occurs at 20 and 60 seconds (arterial and portal venous imaging)

following intravenous contrast administration.

1.2.2 Characteristic Findings of Focal Liver Lesions in Unenhanced- and Gadolinium Chelates-enhanced MR Imaging

1. Benign Liver Tumors

● *Hemangioma:*

Hemangioma is the most common benign hepatic neoplasm, occurring 5% to 20% of the population. Women are affected more than are men and the lesions are commonly found in a subcapsular location in the right lobe of the liver.

On MR images hemangiomas have a characteristic appearance of a 1 cm to 3 cm lesion that is extremely bright ("light bulb") on T2-w images. Lesions larger than 3 cm tend to be less homogeneously bright due to internal fibrous septa or scarring. The tumor margin is well defined, and may be somewhat lobulated. No peritumoral edema is present.

Dynamic MRI with gadolinium chelates administration may display the slow perfusion pattern of hemangioma (i.e., progressive centripetal filling), allowing a differential diagnosis between hemangiomas and primary and secondary malignant tumors.

Three patterns of contrast enhancement are observed in hepatic hemangiomas: (a) uniform enhancement in the arterial phase; (b) peripheral nodular enhancement progressing centripetally to uniform enhancement; (c) peripheral nodular enhancement

with persistent hypointensity centrally. These patterns correlate with the size of the lesions: pattern (a) is seen exclusively in small (< 1.5-cm-diameter) lesions whereas pattern (c) is typical for large, giant hemangiomas.

- *Focal Nodular Hyperplasia (FNH):*

FNH accounts for approximately 8% of all primary hepatic tumors and represents the second most common benign liver tumor after hemangioma. Most FNHs are seen in women in the third to fifth decades of life.

FNH is a well-circumscribed mass, lacking a true capsule, and is characterized by a central scar of vascular connective tissue with prominent arterial vessels that extend outward, through fibrous septa, to the periphery of the tumor.

On precontrast MR images, FNH usually appears isointense with respect to normal liver parenchyma on T1- and T2-w images. The central scar appears hypointense on T1-w images and hyperintense on T2-w images, owing to the presence of connective tissue with rich vascularity.

On dynamic MRI with gadolinium chelates administration, FNH demonstrates peculiar, biphasic enhancement. In the early phase, the central scar is unenhanced, whereas the parenchymal portion of the lesions does enhance, becoming definitely hyperintense with respect to adjacent hepatic parenchyma. After a few minutes, in the delayed phase, the parenchymal portion of the lesion appears almost isointense with respect to the surrounding normal liver, and the uptake of contrast agent by the central scar can be observed, particularily in medium- to large- sized lesions.

- *Hepatocellular Adenoma:*

Hepatocellular adenoma is an uncommon primary benign tumor. The incidence of adenoma increased following the introduction of oral contraceptives, and oral contraceptives and androgen steroid therapy have been identified as definitive causative agents. Hepatocellular adenoma can also occur spontaneously or be associated with underlying metabolic disease. The diagnosis of this entity is clinically important because it can bleed, causing life-threatening hemorrhage, and because it has a potential, although very rare, for malignant transformation.

Hepatocellular adenoma is typically a well-circumscribed tumor. The presence of large subcapsular arterial vessels accounts for its typical hypervascular nature.

The rich intracellular content of glygogen is the main element responsible for the increased signal intensity of hepatocellular adenoma on T1-w images with respect to surrounding liver parenchyma. Areas of internal hemorrhage are typically depicted as markedly hyperintense areas on T1- and T2-w images, owing to the presence of extracellular methemoglobin.

On dynamic contrast-enhanced MR images, hepatocellular adenoma shows early enhancement during the arterial phase, reflecting its hypervascularity, with rapid washout.

1.2.2.2 Malignant Liver Tumors

● *Hepatocellular Carcinoma (HCC):*

HCC is a common malignancy throughout the world, with an estimated incidence of up to 1,000,000 new cases per year. The highest incidence rates are found in sub-Saharan

Africa and the Far East. Areas of low incidence include North America and Northern Europe, whereas Mediterranean countries have an intermediate-to-high incidence. In Western countries and in the Far East, most cases occur in patients with liver cirrhosis, following hepatitis B or C infection.

There are three patterns of HCC in the liver: a solitary mass, a dominant mass with smaller satellite lesions (i.e., multifocal HCC), and diffuse involvement. Most commonly, lesions are well circumscribed with the appearance of a well-defined "capsule".

On MR images, the T1 appearance of HCC ranges from hypointense to slightly hyperintense, depending on fat content, copper deposition within the tumor, and the degree of differentiation. Tumor capsule appears as a low-intensity rim on T1-w images. On T2-w images, most HCC demonstrate increased signal compared to the surrounding liver, although the tumors tend to be inhomogeneous.

HCC is typically nourished by hepatic arterial blood supply. HCC, therefore, typically shows a peak contrast uptake in the arterial phase of the dynamic MR examination. Portal vein thrombosis induced by malignant tumor invasion demonstrates early contrast uptake in the arterial phase like the main tumor, and corresponds to the arteriographic "threads and streaks" sign (i.e. serpiginous or bundle of threads like opacification due to neovascularization of tumor thrombi within the portal vein.).

- *Metastases:*

Metastatic disease to the liver is approximately 20 times more common than is primary hepatic neoplasms. The most common primary tumors to metastasize to the liver are colon, breast, lung, pancreas, melanoma and sarcoma.

The most common appearance of metastatic disease in the liver by MR is round focal lesions with decreased signal on T1-w images and moderately increased signal on T2-w images. Hypervascular metastases are those with an abundant blood supply, typically greater than that of normal liver. These tumors include choriocarcinoma, renal cell carcinoma, thyroid carcinoma, breast carcinoma, melanoma, carcinoid tumor and islet cell tumor. In general, these tumors may have hyperintense signal on T2-w images, and so potentially could be mistaken for hemangioma or cyst. In addition, most of these tumors have an increased tendency to have intratumoral hemorrhage. This results in increased signal on T1-w images as well as T2-w images. Melanoma, due to T1-shortening effect of melanin, shows increased signal on unenhanced T1-w image even if hemorrhage is not present.

With dynamic scanning contrast enhancement of metastases is usually delayed when compared with that of hemangiomas. Moderate peripheral enhancement may be seen with variable but rather slow, irregular enhancement of the central portion of the lesions in most cases, and little or no enhancement in others. Hypervascular metastases may demonstrate early arterial contrast enhancement, but they do not demonstrate the peripheral puddling and tendency toward central filling, which is characteristic of hemangiomas.

- *Cholangiocellular Carcinoma (CCC):*

Intrahepatic CCC is a relatively uncommon neoplasm, although it represents 10% of primary liver tumors and is the second most common primary liver malignancy after HCC.

The MR appearance of CCC is that of a non-capsulated tumor, hypointense on T1-w images and hyperintense on T2-w images. Dilatation of the peripheral portion of the intrahepatic biliary ducts may be seen. The SI of the tumor is variable according to the amount of fibrosis, necrosis, and mucinous material within the tumor. Central hypointensity may be seen on T2-w images, corresponding to central areas of fibrosis.

On dynamic contrast-enhanced MR studies, minimal to moderate peripheral enhancement is evident followed by progressive filling. Diffuse interstitial enhancement within the tumor, reflecting the large amount of fibrotic tissue, is typically seen on delayed MR images.

2. PATIENTS, MATERIALS AND METHODS

2.1 Patients

In this retrospective study 216 consecutive patients, referred for clinical reasons, were examined with ferucarbotran-enhanced MR imaging of the liver during a 14 months period. Of 216 patients, we selected 173 patients with focal liver lesions. All patients gave written informed consent for the examination. Since the examination was part of the clinical routine work-up, no ethic board approval was needed.

Exclusion criteria for SPIO-enhanced liver MR imaging:

• Patient age less than 18 years

• Any contraindication to MR imaging

• Acute hepatitis or serious liver dysfunction

• Severe renal failure

• History of severe adverse events related to drugs or contrast agents

• Pregnancy or lactation in women

• Iron overload

• Injection of an investigational drug within 30 days before the study

• Intravenous administration of contrast material within 24 hours before MR imaging

2.1.1 Study I (T2-weighted FSE and T2*-weighted GRE sequences)

Of 173 patients, 105 were excluded from this study due to missing confirmative diagnosis (n=51), lost imaging data (n=2), severe artifact (n=6) status after TACE (n=17) and inadequate examination (n=29). The remaining 68 patients with a mean age of 61 years (age range, 21-79 years; 19 women, 49 men) were included in this study. The distribution of the different lesions in the study population is given in Table 3.

	Diagnostic Method	
Diagnosis	*Pathological (n=36)	**Follow Up (n=32)
Malignant (n=46)		
HCC (n=29)	21	8
Metastasis (n=15)	8	7
CCC (n=2)	1	1
Benign (n=22)		
Hemangioma (n=6)	1	5
Adenoma (n=5)	3	2
FNH (n=3)	2	1
Cyst (n=8)		8

Table 3: Case distribution in study group I according to confirmative diagnostic method (n=No. of case).
Note- *Pathological confirmation was obtained by fine needle aspiration biopsy (n=25) and surgery (n=11). **The diagnosis was made with clinical and radiological follow-up. CCC; Cholangiocellular Carcinoma, FNH; Focal Nodular Hyperplasia, HCC; Hepatocellular Carcinoma

2.1.2 Study II (T1-weighted early dynamic GRE sequences)

Of 173 patients, 113 were excluded from this study due to missing confirmative diagnosis (n=69), lost imaging data (n=2), severe artifacts (n=4), status after TACE (n=17) and because the dynamic examination was not performed (n=21). The remaining 60 patients with a mean age of 61.2 years (age range, 21-79 years; 17 women, 43 men) were included in this study.

The distribution of the different lesions in the study population is given in Table 4.

Diagnosis	Diagnostic Method	
	*Pathological (n=32)	**Follow Up (n=28)
Malignant (n=41)		
HCC (n=25)	17	8
Metastasis (n=14)	7	7
CCC (n=2)	1	1
Benign (n=19)		
Hemangioma (n=6)	1	5
Adenoma (n=3)	3	
FNH (n=3)	3	
Cyst (n=7)		7

Table 4: Case distribution in study group II according to confirmative diagnostic method.
*Note- *Pathological confirmation was obtained by fine needle aspiration biopsy (n=23) and surgery (n=9).** The diagnosis was made with clinical and radiological follow-up.*
CCC; Cholangiocellular Carcinoma, FNH; Focal Nodular Hyperplasia, HCC; Hepatocellular Carcinoma

The T1-w dynamic studies were performed with 2D-GRE sequences in 23/60 during the first 9 months and with 3D-GRE VIBE (Volumetric Interpolated Breath-hold Examination) sequences in 37/60 patients during the following 5 months of the study interval. The change from the 2D-GRE to the 3D-GRE sequences was due to a change of the sequences in the routine liver MR protocol.

The distribution of the cases according to each sequence is shown in Table 5.

Diagnosis	Sequence for dynamic imaging	
	2D-GRE (n=23)	3D-GRE VIBE (n=37)
HCC (n=25)	16	9
Metastasis (n=14)	4	10
CCC (n=2)	1	1
Hemangioma (n=6)	2	4
Adenoma (n=3)		3
FNH (n=3)		3
Cyst (n=7)		7

Table 5: Case distribution according to T1-weighted GRE dynamic MRI Sequences

● Diagnostic Criteria with Clinical and Radiological Follow-up:

With clinical and radiological follow-up, diagnosis of liver metastasis was made on the basis of surgically proven primary tumor, increased levels of serum tumor marker, and tumor growth on follow-up sonography, CT and/or MR imaging. Lesions were diagnosed as HCC if they had underlying liver cirrhosis, showed typical imaging findings on CT, sonography and angiography, and increased levels of serum α-fetoprotein. Lesions were diagnosed as adenoma if they presented as hyperintense lesions on T1-w MR image, showed strong arterial enhancement with rapid wash out on dynamic CT or MRI and no increase in size for 6 months and in the case of patients suffering from underlying glycogen storage disease. Lesions were diagnosed as FNH if they showed nearly same density or SI as the normal liver parenchyma on CT and MR images, presented with a central scar that showed bright SI on T2-w MR images and did not exhibit increase in size for 6 months. Lesions were diagnosed as hemangioma if they were well-marginated hyperechoic masses at sonography, showed dense peripheral

nodular enhancement in the arterial phase with subsequent centripetal fill-in on contrast-enhanced CT or MR images, were markedly hyperintense on prior T2-w MR images and showed no increase in size for 6 months. Lesions were diagnosed as cysts if they showed HU values of 0-15 and no enhancement on contrast-enhanced CT scans or were anechoic with posterior sonic enhancement at sonography.

2.2 Contrast Agent

The liver-specific SPIO ferucarbotran (Resovist™, Schering, Germany) was used. Before each examination, an intravenous catheter was placed in an arm vein and attached through a connecting line to a 20-ml syringe to prevent the patient from changing position during examination. Patients up to 60 kg body weight received 0.9 ml ferucarbotran and patients above 60 kg body weight received 1.4 ml ferucarbotran. Ferucarbotran was administered through a 5 μm filter carefully into the connecting tube by hand then injected rapidly as an intravenous bolus by hand together with a 20-ml saline flush.

2.3 MR Imaging Method

MR imaging studies were performed at 1.5-T high performance gradient systems (Sonata and Symphony Quantum, Siemens, Erlangen, Germany), using a phased array body coil.

2.3.1 Study I (T2-weighted FSE and T2*-weighted GRE sequences)

After non-enhanced (NCE) T2-w FSE images were obtained, contrast-enhanced (CE) T2-w FSE images 10 min after bolus injection were obtained, followed by CE- T2*-w GRE images. NCE- T2*-GRE images were not obtained

Imaging parameters for T2-w FSE and T2*-GRE sequences are shown in Table 6.

	T2-w FSE sequence	T2*-w GRE sequence
TR (msec)/TE (msec)/flip angle	2800/125	117/100/30°
Section thickness/gap	6 mm/0.6	6 mm/0.6
Matrix	256×256	256×256
Field of view	300-400	300-400
Fat saturation	(+)	(-)
Breath hold	(+)	(+)

Table 6: Parameters for T2-weighted FSE and T2*-weighted GRE sequences

2.3.2 Study II (T1-weighted early dynamic GRE sequences)

Axial T1-w dynamic imaging was obtained before, and 20, 50 and 120 seconds after bolus injection of ferucarbotran.

Imaging parameters for T1-w 2D-GRE and T1-w 3D-GRE VIBE sequences are shown in Table 7.

	2D-GRE sequence	3D-GRE sequence
TR (msec)/TE (msec)/flip angle	174/4.76/70°	4.45/1.54/15°
Section thickness/gap	8 mm/0.8	4 mm/0
Matrix	256×256	256×192
Field of view	300-400	300-400
Fat saturation	(-)	(+)
Breath hold	(+)	(+)

Table 7: Parameters for T1-weighted 2D-GRE and T1-weighted 3D-GRE VIBE sequences

2.4 Quantitative Image Analysis

On a picture archiving and communication system (PACS, Magic View 1000, Erlangen, Germany), one radiologist performed operator-defined region-of-interest (ROI) measurements.

2.4.1 Study I (T2-weighted FSE and T2*-weighted GRE sequences)

The ROI measurements were performed for the SI of liver parenchyma (in regions free of artifacts and of large blood vessels) and focal liver lesions (excluding central necrosis or scar) and background noise on NCE- and CE- T2-w FSE and CE-T2*-GRE images.

2.4.2 Study II (T1-weighted early dynamic GRE sequences)

The ROI measurements were performed for the SI of liver parenchyma (in regions free of artifacts and large blood vessels), portal vein, aorta, inferior vena cava (IVC) and focal liver lesions (excluding central necrosis or scar) and background noise before and after injection of the contrast agent.

● ROI measuring methods:

ROIs were placed in the same anatomic area with the same size and shape on both NCE- and CE- images. For the measurement of SI of liver tissue and aorta, three separate ROIs from different areas were measured, and the results were averaged. For the measurement of SI of IVC and portal vein, only one ROI was measured. For the hepatic lesions, circular ROIs were drawn to encompass as much of the lesion as possible. If the focal lesion was totally inhomogeneous in SI, two separate ROIs from high and low SI areas were measured and the results were averaged. If the lesion was inhomogeneous with different SI in the center and the rim, the SI of the rim was chosen, since it defines the contrast to the liver parenchyma. If multiple lesions were present in a patient, a single lesion of the largest size and best representing the lesions type was chosen and ROIs were measured. If different lesion types were present in a patient, we preferred solid malignant lesions to solid benign and cystic lesions. Background noise was measured in ROIs as large as possible ventrally to the liver outside the patient along the phase-encoding axis, avoiding ghosting artifacts that might have propagated over the image.

● Signal-to-noise ratio (SNR) and contrast-to-noise ratio (CNR):

$$SNR = \frac{\text{Signal Intensity of liver or lesion}}{\text{Standard Deviation of background noise}}$$

$$CNR = \frac{\text{Signal Intensity of lesion} - \text{Signal Intensity of liver}}{\text{Standard Deviation of background noise}}$$

• The percentage of signal intensity loss (PSIL) of the lesion in CE-T2-w FSE images:

$$PSIL = \frac{\text{SNR precontrast} - \text{SNR postcontrast}}{\text{SNR precontrast}} \times 100$$

• <u>Statistical Analysis</u>:

In study group I, the statistical significance of the difference in SNR, CNR and PSIL between the lesions and between the imaging sequences was evaluated by means of the paired t-test. Sensitivity and specificity for the differentiation of benign and malignant lesions were calculated with the different threshold PSIL of 20%, 25% and 30%.

In study group II, the change in SNR and CNR between unenhanced and 20 second phased images in each organ and lesion was evaluated by means of the paired t-test, and difference between different patients groups by means of the unpaired t-test.

P-values less than or equal to 0.05 were considered statistically significant.

Statistical analysis was performed with SPSS 12.0 (Statistical Package for the Social Science; SPSS Inc., Chicago, Illinois).

2.5 Qualitative Analysis

2.5.1 Study I (T2-weighted FSE and T2*-weighted GRE sequences)

On a PACS two radiologists experienced in liver MR imaging visually evaluated the two image sequences (CE-T2-w FSE and CE-T2*-w GRE) for each case and made a consensus for the following categories:

- Overall image quality

- Lesion conspicuity

- Vessel conspicuity

- Imaging artifacts

- Detected lesion number

- Additional findings (which may be useful in characterization of focal liver lesions); portal vein thrombosis, mosaic pattern in the tumor, tumor capsule, central scar, high SI rim outside the tumor

The criteria for the assessment of overall image quality were visual quality of the liver margin, depiction of the vascular structures, and homogeneity of the SI in liver parenchyma and presence of image artifacts.

- <u>Statistical Analysis</u>

The two image sequences were compared for each category and scored as follows: CE-T2-w FSE superior, CE-T2*-w GRE superior, equal, or not identified. In each category, the cases scored as "equally" or "not identified" were discarded, and the remaining cases were tested for statistical significance by means of Chi-square and Fischer exact tests. The results were considered significant at $p < .05$.

2.5.2 Study II (T1-weighted early dynamic GRE sequences)

Two radiologists visually evaluated the dynamic enhancement pattern of the different lesions over time and made a consensus to find out whether characteristic enhancement pattern existed that might be equivalent to known enhancement pattern from gadolinium-enhanced dynamic MRI. Hypo- or hyperintensity was defined as lower or higher SI of the lesion in comparison to the adjacent liver parenchyma.

3. RESULTS

3.1 Study I (T2-weighted FSE and T2*-weighted GRE sequences)

3.1.1 Quantitative Analysis

• *SNR and CNR:*

The mean SNR of the liver and focal lesions on each imaging sequence are shown in Graph 1.
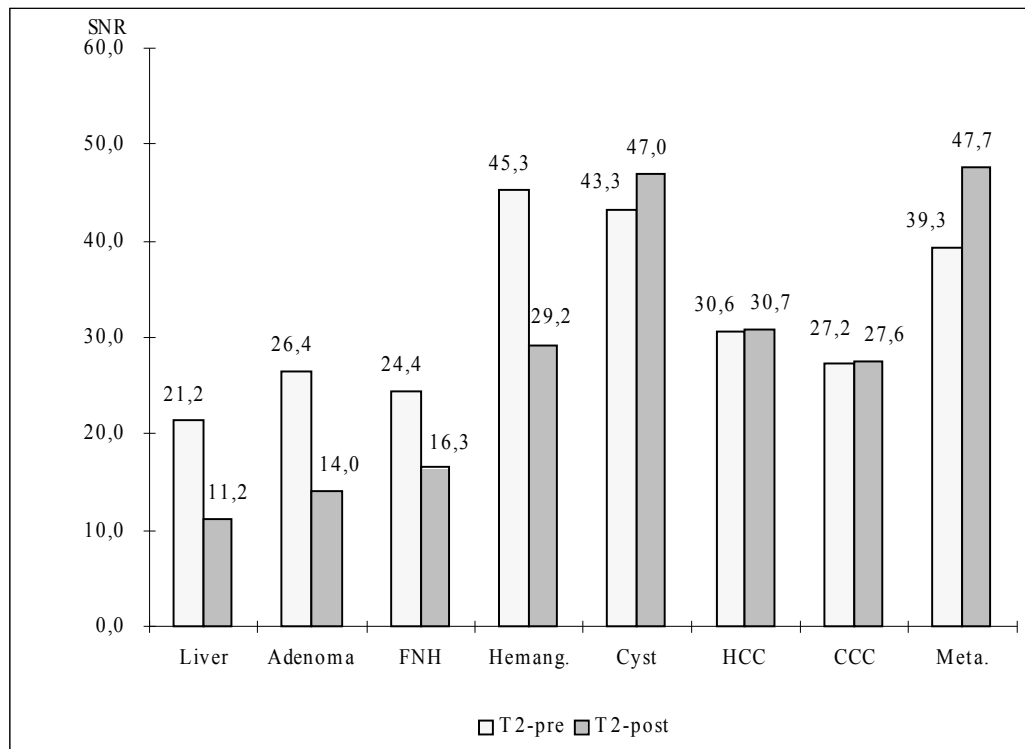
Graph 1. SNR of the liver and focal liver lesions at pre- and post- contrast enhanced T2-weighted FSE and post-contrast enhanced T2*-weighted GRE images.
Note- CCC; Cholangiocellular Carcinoma, FNH; Focal Nodular Hyperplasia, HCC; Hepatocellular Carcinoma

The SNR of the liver significantly decreased from 21.2 on NCE-T2-w FSE images as compared with 11.2 on CE-images (p< .05). The mean SNR of solid benign lesions showed a decrease from 34.1 to 21.0 (p< .05). In malignant lesions, the mean SNR showed only a minor decrease from 33.3 to 32.5 (n.s.).

The statistical significance in the difference of SNR between the lesion types on each imaging sequence is shown in Table 8.

|	Adenoma vs FNH	Hemangioma vs HCC	Hemangioma vs Metastasis	Cyst vs HCC	Cyst vs Metastasis	HCC vs Metastasis
NCE-T2-w FSE	NS	< .05	NS	< .05	NS	NS
CE-T2-w FSE	NS	NS	< .05	NS	NS	< .05
CE-T2*-w GRE	< .05	NS	NS	< .05	< .05	NS

Table 8. Statistical significance of the difference in SNR between the lesion types (p-value).
Note.- < .05: statistically significant ; NS: statistically not significant
CCC; Cholangiocellular Carcinoma, FNH; Focal Nodular Hyperplasia, HCC; Hepatocellular Carcinoma

The mean CNR of focal lesions in comparison to the adjacent liver parenchyma on each imaging sequence is shown in Graph 2. The mean CNR of the malignant lesions was the highest in the CE-T2*-w sequence as compared to the CE- and the NCE- T2-w FSE sequence (29.9 vs. 22.7 (p< .01) vs. 12.8 SI (p< .01)). The mean CNR of adenoma and cyst were statistically significantly lower than those on CE-T2-w FSE images (p < .05).

CNR
40,0
35,0
30,0
25,0
20,0
15,0
10,0
5,0
0,0
-5,0

7,5   -0,6   -1,1   Adenoma
1,2   7,8   18,0   FNH
25,6   19,3   30,4   Hemang.
24,0   31,9   11,8   Cyst
10,4   19,6   28,8   HCC
13,6   18,3   20,3   CCC
15,6   35,5   29,1   Meta.

□ T2-pre   ▨ T2-post   ▨ T2*-post
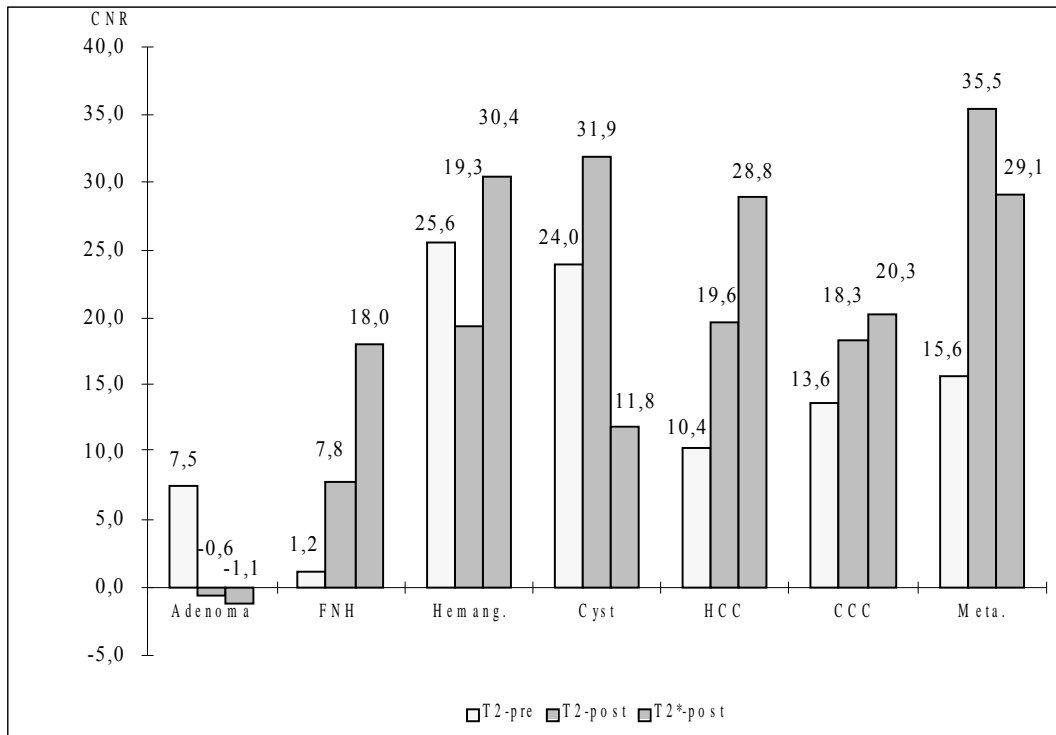
Graph 2. CNR of focal liver lesions at pre- and post- contrast enhanced T2-weighted FSE and post-contrast enhanced T2*-weighted GRE images.

Note- CCC; Cholangiocellular Carcinoma, FNH; Focal Nodular Hyperplasia, HCC; Hepatocellular Carcinoma

The statistical significance in the difference of CNR between the lesion types on each imaging sequence is shown in Table 9.

	Adenoma vs FNH	Hemangioma vs HCC	Hemangioma vs Metastasis	Cyst vs HCC	Cyst vs Metastasis	HCC vs Metastasis
NCE-T2-w FSE	NS	< .05	< .05	< .05	< .05	NS
CE-T2-w FSE	NS	NS	NS	< .05	NS	NS
CE-T2*-w GRE	< .05	NS	NS	< .05	< .05	NS

Table 9. Statistical significance of the difference in CNR between the lesion types (p-value).

Note- < .05: statistically significant; NS: statistically not significant

CCC; Cholangiocellular Carcinoma, FNH; Focal Nodular Hyperplasia, HCC; Hepatocellular Carcinoma

• *PSIL:*

The mean PSIL (90% Confidence Intervals) of each lesion type were as follows: Adenoma 46.9% (38.8% to 55.0%), FNH 33.0% (21.3% to 44.7%), hemangioma 35.3% (26.9% to 43.8%), HCC 3.1% (−1.4% to 7.6%), Metastasis 4.0% (−1.4% to 9.5%), CCC −1.7% (−22.3% to 18.8%). The PSIL of non-cystic benign lesions (mean PSIL 39.6%) were statistically significantly higher as compared to that of malignant lesions (mean PSIL 3.2%). The distribution of PSIL of each focal liver lesion (14 non-cystic benign and 46 malignant lesions) is shown in Graph 3.
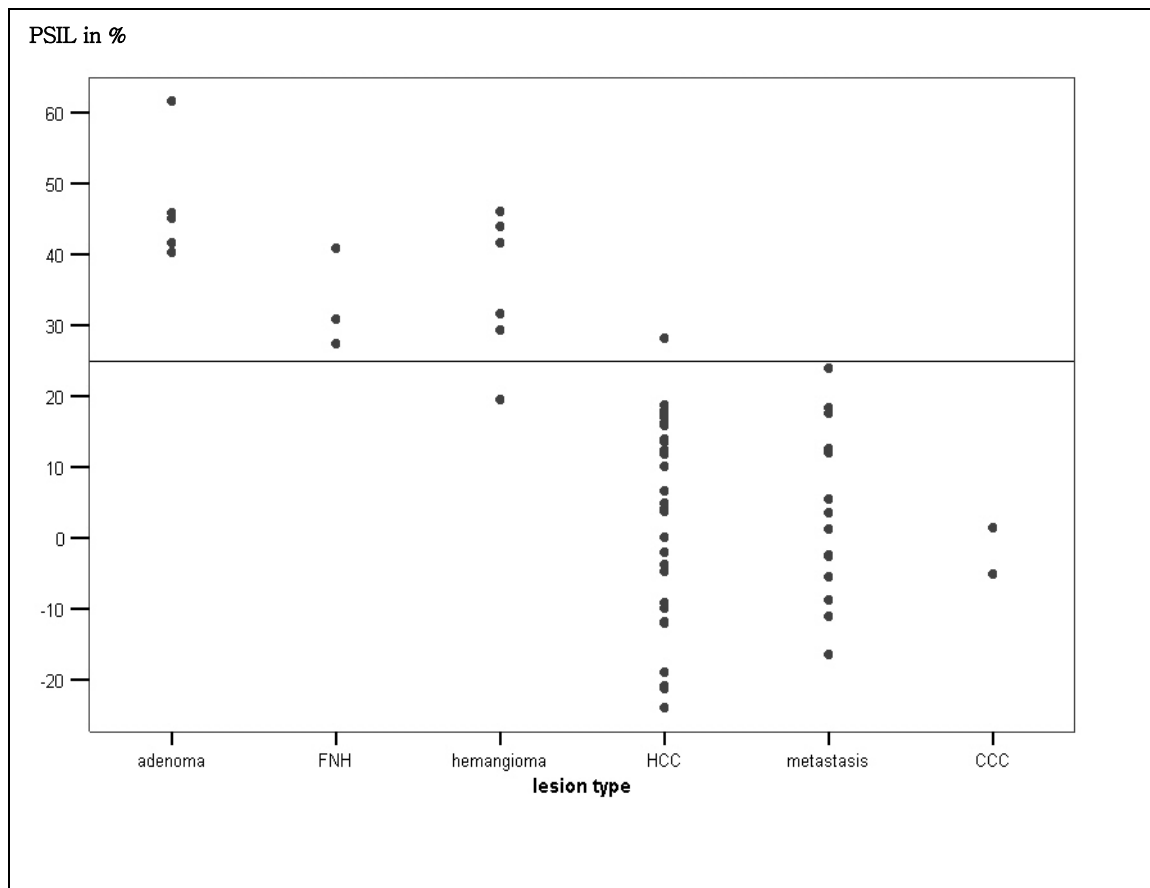
Graph 3. Percentage of signal intensity loss (PSIL) in noncystic benign (n=14) and malignant lesions (n=46) on T2-weighted FSE sequences after ferucarbotran administration.

Note- CCC; Cholangiocellular Carcinoma, FNH; Focal Nodular Hyperplasia, HCC; Hepatocellular Carcinoma

When the threshold PSIL for the differentiation of benign and malignant lesions was determined at 25%, 45 of 46 malignant lesions and one of 14 benign lesions showed a PSIL lower than 25%, resulting in a sensitivity and specificity for the characterization of malignant lesions of 97.8% and 92.9%. The malignant lesion with a PSIL higher than 25% was a HCC (PSIL 28.1%), and the benign lesion with a PSIL lower than 25% was a hemangioma (PSIL 19.5%).

When the threshold was determined at 30%, 46 of 46 malignant lesions and 3 of 14 benign lesions showed a PSIL lower than 30%, resulting in a sensitivity and specificity for the characterization of malignant lesions of 100% and 78.6%. When the threshold was determined at 20%, 44 of 46 malignant lesions and 1 of 14 benign lesions showed a PSIL lower than 20%, resulting in a sensitivity and specificity for the characterization of malignant lesions of 95.7% and 92.9%

3.1.2 Qualitative Analysis

The results of visual comparison of two image sequences (CE-T2-w FSE and CE-T2*-w GRE) are shown in Table 10. CE-T2*-w GRE images were superior to CE-T2-w FSE images with statistical significance in the categories of overall image quality, lesion

conspicuity and vessel conspicuity ($p < .05$). Imaging artifacts were more frequently shown on the CE-T2-w FSE images than CE-T2*-w GRE images with statistical significance ($p < .05$). In the categories of additional findings no significant difference between the two sequences was noted ($p > .05$).

Category	T2-w FSE superior	T2*-w GRE superior	Equally rated	N	p-value
Overall Image Quality	7	44	17	NA	< .05
Lesion Conspicuity	[a]16	40	12	NA	< .05
Vessel Conspicuity	1	49	18	NA	< .05
Artifact	28	7	6	27	< .05
Detected Lesion Number	[c]7	11	14	[b]35	NS
Additional Findings					
Portal Vein Thrombosis	2	1	4	61	NS
Mosaic Pattern	5	1	1	61	NS
Capsule	2	3	1	62	NS
Central Scar	1	0	1	66	NS
Peripheral rim	1	5	0	62	NS

Table 10. Comparison of image scores for contrast-enhanced T2-weighted FSE versus T2-weighted GRE sequences*
Note- Numbers in the T2-w FSE and T2-w GRE columns indicate the number of cases in which each of the sequences was rated superior. Equally rated = numbers of cases for which the T2-w FSE and T2*-w GRE sequences were rated equal, N = number of cases in which a finding was not identified with either sequences, NA = not applicable, NS = not significant.*
[a] Eight of them were cyst.
[b] Five of them had too numerous focal lesions to count.
[c] Six of them were benign lesions (one FNH, 3 cyst, 2 Hemangioma).

● *Lesion Conspicuity (Table 11):*

In general, overall image quality and imaging artifacts affected the lesion conspicuity (Figure 2). The superiority of lesion conspicuity on CE-T2*-w GRE images was caused by markedly negative (adenoma) or positive (HCC) CNR in adenoma and HCC. In cysts the CNR on CE-T2*-w GRE images was markedly decreased in contrast to the bright signal intensity on CE-T2-w FSE images resulting in inferiority of lesion conspicuity.

	T2-w FSE superior	T2*-w GRE superior	Equally rated
Adenoma (n=5)	0	5	0
FNH (n=3)	1	2	0
Hemangioma (n=6)	3	3	0
Cyst (n=8)	8	0	0
HCC (n=29)	1	24	4
Metastasis (n=15)	1	10	4
CCC (n=2)	0	1	1

Table 11. Lesion conspicuity according to the lesion types.
Note- Numbers in the T2-w FSE and T2*-w GRE columns indicate the number of cases in which each of the sequences was rated superior. Equally rated = numbers of cases for which the T2-w FSE and T2*-w GRE sequences were rated equal.
CCC; Cholangiocellular Carcinoma, FNH; Focal Nodular Hyperplasia, HCC; Hepatocellular Carcinoma

● *Imaging Artifacts:*

The imaging artifacts found on CE-T2-w FSE images were motion artifacts in 33 of 68 cases (48.5%) and ghosting artifacts from the GB in one case. In eight patients the artifacts were severe enough to degrade the image quality with blurring of liver and lesion margins; in those eight patients seven suffered from a large amount of ascites (Figure 1). The imaging artifacts arising on CE-T2*-w GRE images were ghosting artifacts in 8 of 68 cases (11.8%), seven from the aorta and one from the IVC, metallic artifacts in 3 cases, and motion artifacts and other type in each one. In each one case the ghosting artifacts arising from the aorta and the metallic artifacts obscured a focal liver lesion directly (Figure 2). In 4 cases the ghosting artifacts from the aorta were mimicking a focal lesion in left hepatic lobe. The metallic artifacts (n=3) were arising from the anterior abdominal wall, from surgical clips at the margin of right hepatic lobe after liver resection and from surgical material in the vertebral column in each one case. Although these artifacts were also shown on CE-T2-w FSE images, they did not affect significantly the image quality or lesion conspicuity on CE-T2-w FSE.

● *Adenoma:*

All adenomas (n=5) showed very dark SI on CE-T2*-w GRE images being hypointense to the surrounding liver parenchyma. Two cases showed isointense SI with central foci of high SI mimicking FNH on CE-T2-w FSE images. These lesions could be differentiated from FHN due to very dark SI of the lesions on CE-T2*-w GRE images (Figure 3).

Three patients had multiple adenomas. In two patients, the number of detected lesions were higher on CE-T2*-w GRE images rather than CE-T2-w FSE due to the marked

negative CNR on CE-T2*-w GRE images. One case excluded due to too numerous focal lesions to count.

● *FNH:*

FNH were slightly hyper- or iso- intense on CE-T2-w FSE and CE-T2*-w GRE images. Two cases had a central scar. One case showed the central scar on CE-T2-w FSE image only, but not on CE-T2*-w GRE image (Figure 4). Another case of FNH showed the central scar on both image sequences, although it presented higher SI on the CE-T2-w FSE image.

● *Hemangioma:*

Hemangioma presented in five of six cases with high SI on CE-T2-w FSE and CE-T2*-w GRE images with no visually noticeable change in SI after ferucarbotran administration. One hemangioma exhibited a visually noticeable signal decrease in the ferucarbotran-enhanced images.

A case of hemangioma combined multiple simple cysts. Both lesion types presented with bright SI on NCE-T2-w FSE images. Hemangioma showed signal decrease on both CE-T2-w FSE and CE-T2*-w GRE images as compared to NCE- T2-w FSE images. In contrast, cyst presented with bright SI on CE- T2-w FSE as well as NCE-T2-w FSE images and worsened lesion conspicuity due to decreased CNR on CE-T2*-w GRE images.

● *HCC and Metastases:*

HCC showed variable SI on NCE- and CE- T2-w FSE images and high SI with highest CNR on CE- T2*-w GRE images (Figure 5). Metastases showed high SI with or without an internal heterogeneous area on both sequences (Figure 6). In each one patient HCC and metastasis presented combined with simple cysts. In these cases, the differentiation between the malignant lesion and the cyst was easier on CE-T2*-w GRE images rather than CE-T2-w FSE images due to the marked difference of SI and CNR between the two lesion types.

The results of the visual evaluation of the morphological features, such as portal vein thrombosis, central scar, mosaic pattern and dark SI capsule, which may be useful for the characterization of focal lesions, are shown in Table 10. These findings showed no statistically significant difference between two image sequences. Mosaic pattern only showed the tendency toward a better visualization on CE-T2-w FSE images ($p > .05$) (Figure 5). A peripheral hyperintense rim outside the tumor could be delineated in 3 of 29 cases of HCC and 3 of 25 cases of metastases. In the assessment of this finding CE-T2*-w GRE images were superior in five cases (n.s.) (Figure 6). In twenty-three patients multiple malignant liver lesions were present. In eight of these cases more focal lesions were detected on CE-T2*-w GRE images. In one case, more focal lesions were detected on CE-T2-w FSE images. Ten cases showed the same number of detected lesions on both image sequences. Four cases were excluded due to too numerous focal lesions to count.

3.2 Study II (T1-weighted early dynamic GRE sequences)

3.2.1 Quantitative Analysis

3.2.1.1 T1-weighted 2D-GRE Dynamic MR Image

● *SNR and CNR Change in Liver and Vascular Structures:*

In the evaluation of liver and vessel SI all vascular structures (IVC and portal vein) showed a negative CNR to the liver parenchyma until 50 seconds after contrast injection (i.e. the vascular structures were hypointense to the liver) (Graph 4).
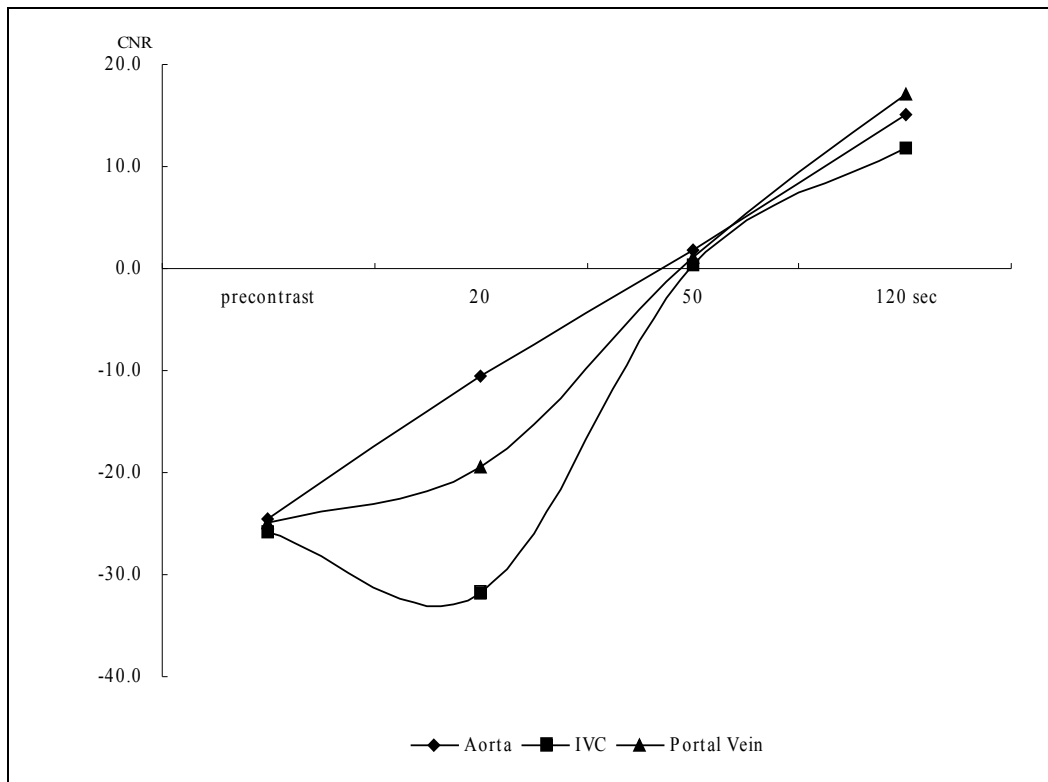
Graph 4. Change in mean CNR of the vascular structures on dynamic T1-weighted 2D-GRE MRI (n=23) after bolus-injection of ferucarbotran.
Note- IVC; Inferior Vena Cava

● SNR and CNR Change in Focal Liver Lesions (Graph 5, 6):

In the group of benign lesions hemangioma (n=2) showed a negative CNR after 20 and 50 seconds and a positive CNR (8.9 ± 26.1) after 120 seconds.

In the evaluation of malignant lesions the SNR in HCC and metastasis increased rapidly 20 seconds after injection. The early increase in SNR was statistically significant ($p < .05$). Nevertheless, HCC, metastasis and CCC showed a negative mean CNR at all time points.
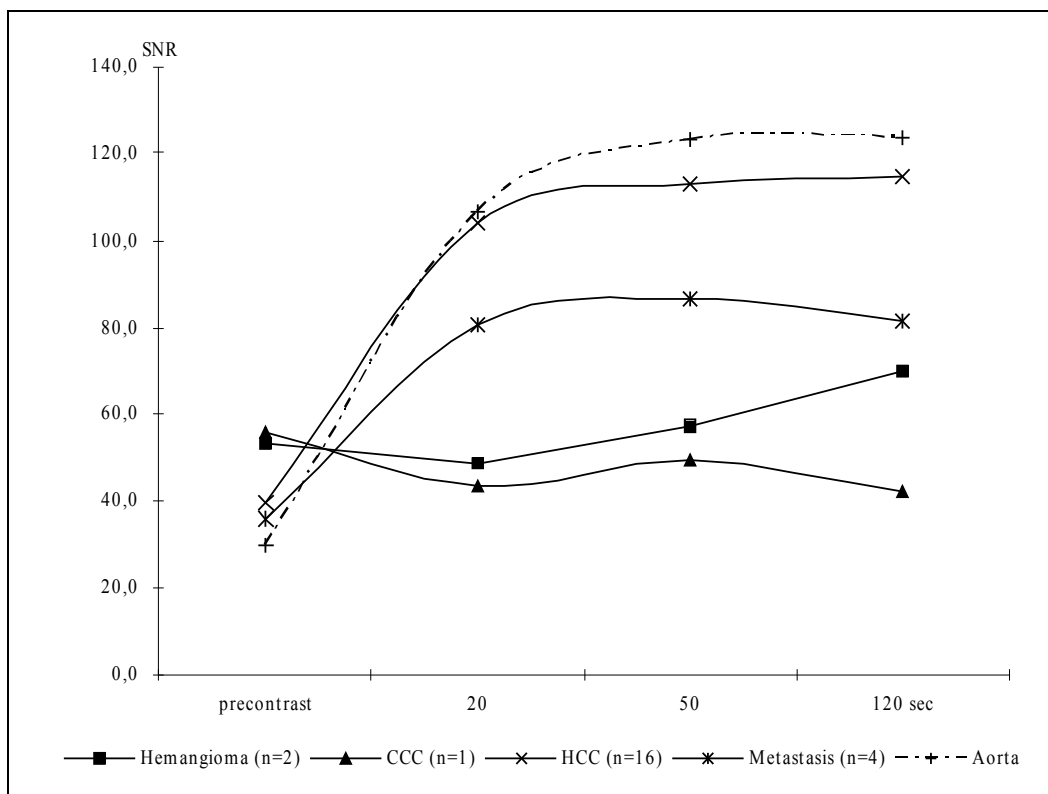
Graph 5. Change in mean SNR of focal liver lesions on dynamic T1-weighted 2D-GRE MRI (n=23).
Note- CCC; Cholangiocellular Carcinoma, HCC; Hepatocellular Carcinoma
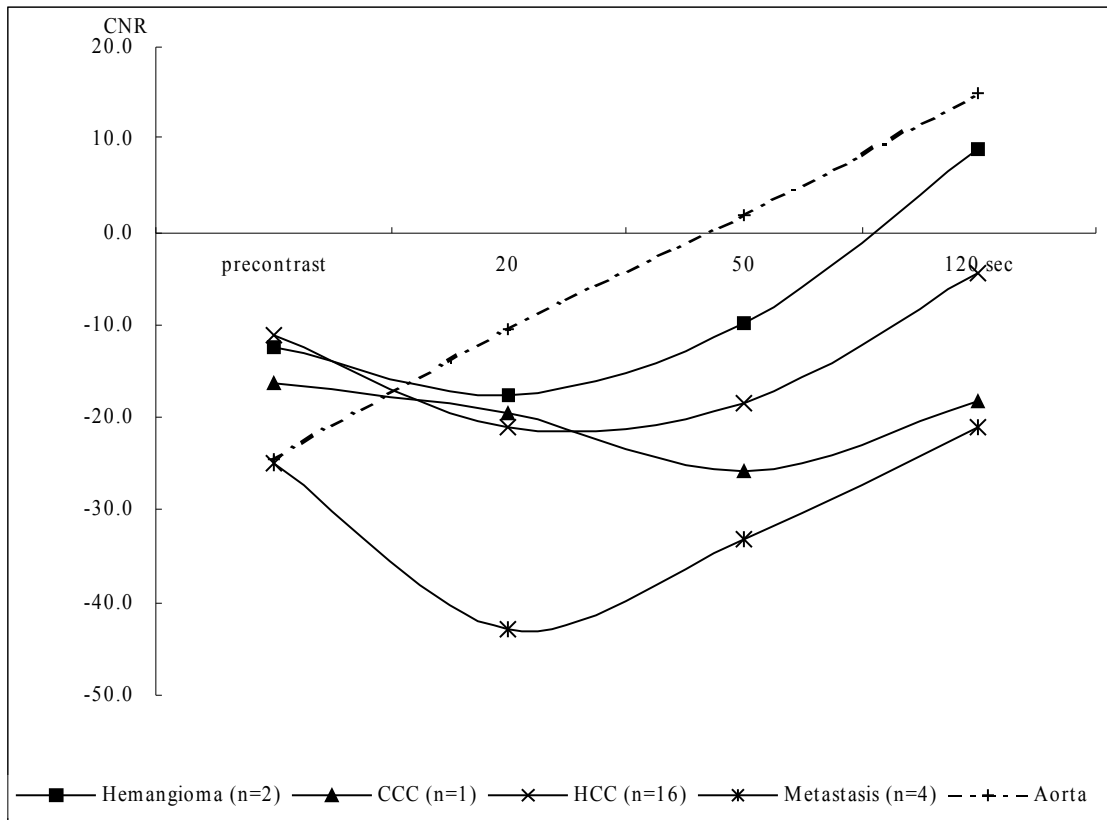
Graph 6. Change in mean CNR of focal liver lesions on dynamic T1-weighted 2D-GRE MRI (n=23).
Note- CCC; Cholangiocellular Carcinoma, HCC; Hepatocellular Carcinoma

3.2.1.2 T1-weighted 3D-GRE Dynamic MR Image

● *SNR and CNR Change in Liver and Vascular Structures:*

In the evaluation of liver and vessel SI all vascular structures (aorta, IVC and portal vein) had statistically significantly increased CNR to the liver parenchyma after 20 seconds ($p < .05$) in comparison to precontrast, and showed positive values at all time points after injection (i.e. the vascular structures were hyperintense to the liver) except

for IVC after 20 seconds (-2.2 ± 20.1) (Graph 7).
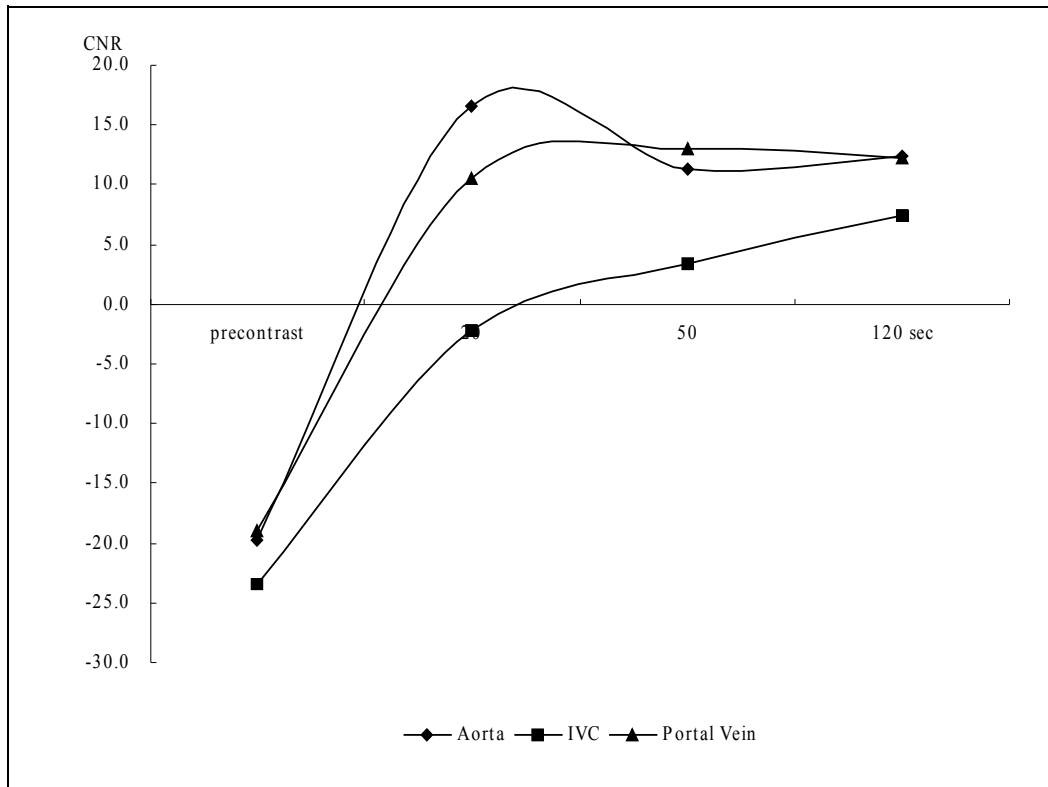
Graph 7. Change in mean CNR of the vascular structures on dynamic T1-weighted 3D-GRE VIBE MRI (n=37)
Note- IVC; Inferior Vena Cava

● *SNR and CNR Change in Focal Liver Lesions (Graph 8, 9) :*

For benign lesions the SNR and accordingly the CNR were highest in adenomas and lowest in cysts at all time points. In hemangioma the CNR changed from negative (-7.6 ± 18.0) at precontrast to positive (9.1 ± 35.4) at 20 seconds after injection and then persisted positive on subsequent phases. The CNR in FNH remained unchanged with a value of more or less zero at all time points (-2.0 ± 6.2; 2.6 ± 24.6; 0.8 ± 22.9; 2.5 ± 17.2).

The SNR and CNR in malignant solid lesions (HCC, metastases and CCC) was below those of benign noncystic lesions (adenoma, FNH, hemangioma) at all time points after injection, but this difference was not statistically significant ($p > .05$). The CNR of malignant solid lesions was negative at all time points; however it was higher than that of cysts.

The change in CNR in all benign and malignant lesions after 20 seconds in comparison to precontrast was statistically not significant ($p > .05$).
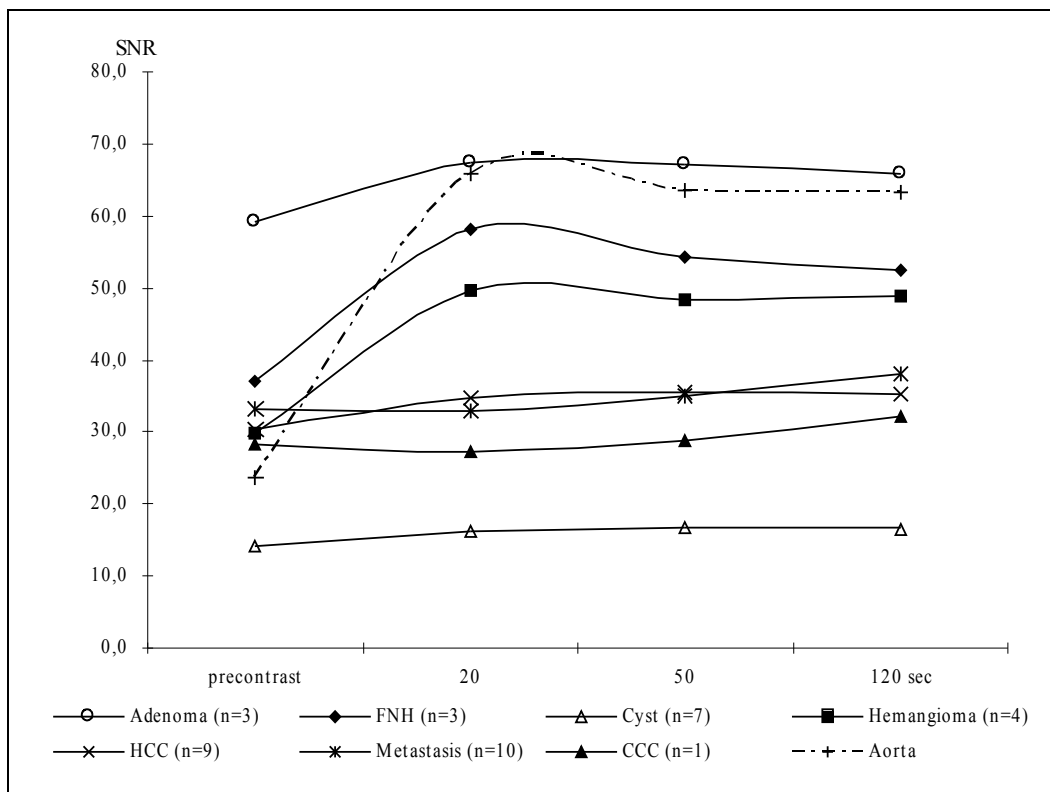
Graph 8. Change in mean SNR of focal liver lesions on dynamic T1-weighted 3D-GRE VIBE MRI (n=37).
Note- CCC; Cholangiocellular Carcinoma, FNH; Focal Nodular Hyperploasia, HCC; Hepatocellular Carcinoma
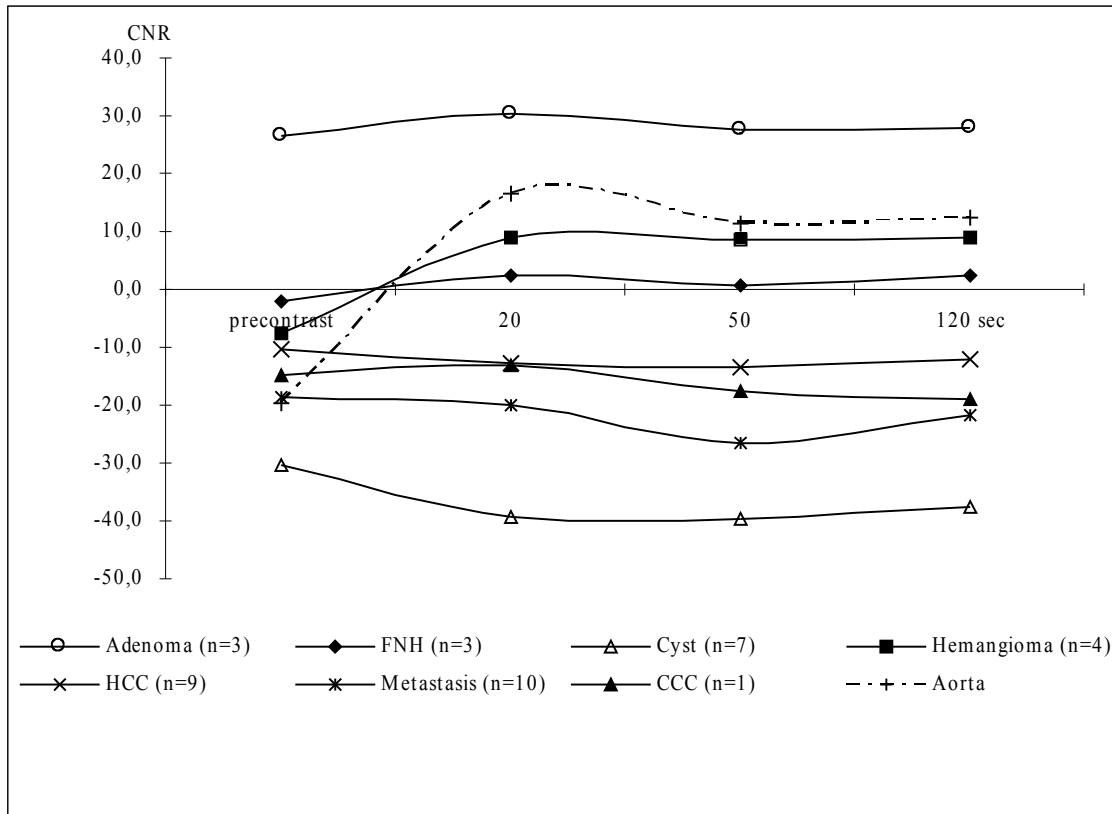
Graph 9. Change in mean CNR of focal liver lesions on dynamic T1-weighted 3D-GRE VIBE MRI (n=37).
Note- CCC; Cholangiocellular Carcinoma, FNH; Focal Nodular Hyperploasia, HCC; Hepatocellular Carcinoma

3.2.2 Visual Evaluation

3.2.2.1 T1-weighted 2D-GRE Dynamic MR Image

● *Hemangioma:*

Hemangioma revealed hypointensity at precontrast and after 20 seconds. The SI then

gradually increased with a centripetal fill-in enhancement and slight hyperintensity after 120 seconds.

● *HCC:*

Seven of 16 HCCs exhibited no significant SI change at all time points after injection as compared with precontrast images (Figure 7). Six cases exhibited gradual enhancement with hypointensity at precontrast and after 20 seconds and iso- or slightly hyperintensity after 50 and 120 seconds. Two HCCs showed decreasing enhancement with isointensity after 20 seconds and hypointensity after 50 and 120 seconds.

● *Metastasis:*

In 2/4 metastases hypointensity at all time points were observed, the remaining 2 cases showed gradual enhancement with hypointensity at 20 seconds phase and isointensity at 120 seconds phase. Two metastases showed ring enhancement outside the tumor margin at 120 seconds phase (Figure 8).

3.2.2.2 T1-weighted 3D-GRE Dynamic MR Image

● *Adenoma:*

All adenomas (n=3) presented with hyperintensity (Figure 9) with sharp margins with no change over time.

● *FNH:*

All FNHs (n=3) were almost isointense at all time points with only slight variations. Two FNHs had an internal scar. One internal scar showed gradually increased enhancement after injection, the other remained hypointense (Figure 10).

• *Hemangioma:*

In hemangioma two of 4 cases displayed nodular centripetal fill-in enhancement (Figure 11), the remaining two cases showed homogenously increasing SI without nodular appearance.

• *HCC:*

Seven of 9 HCCs showed no significant change in SI at all time points with hypointensity in 4 cases, and isointensity, slight hyperintensity and mixed SI in each one. Two of 9 HCCs showed slight early enhancement and slight wash out. One HCC presented with ring enhancement outside the tumor margin after injection (Figure 12).

• *Metastasis:*

In 9/10 metastases no significant SI change was observed at all time points with hypointensity in 8 cases and mixed SI in one. One of 10 metastases showed isointensity after 20 seconds and hypointensity at the other 2 phases.

4. Figures

4.1 Overview

Study I (T2-weighted TSE and T2*-weighted GRE sequences)

Study II (T1-weighted early dynamic GRE sequences)

Figure 1:

1.1

1.2

1.3

Artifacts due to motion in a case of hepatocellular carcinoma.

1.1 Unenhanced-, and **1.2** Ferucarbotran-enhanced T2-weighted FSE images show poor image quality and poor lesion conspicuity. **1.3** Ferucarbotran-enhanced T2*-weighted GRE image shows good image quality with good lesion and vessel conspicuity. The HCC in left hepatic lobe (arrow) is not obvious in **1.1** and **1.2**.

Figure 2:
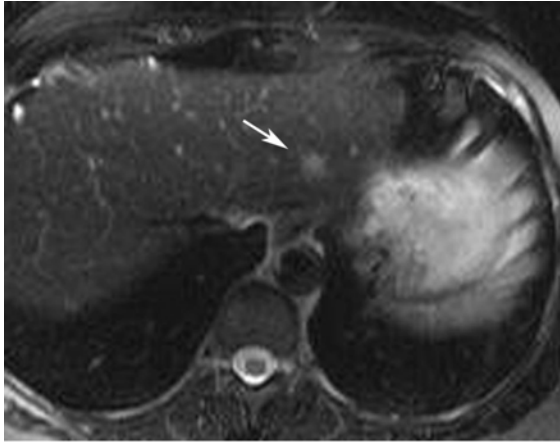
2.1
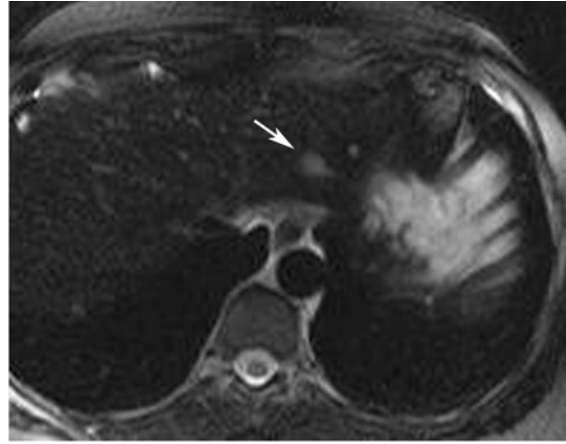
2.2
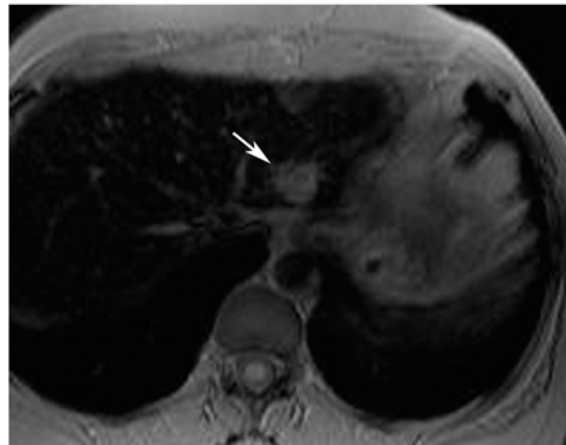
2.3

Ghosting artifacts in a case of hemangioma.

2.1 Unenhanced-, **2.2** Ferucarbotran-enhanced T2-weighted FSE images show a small high signal intensity hemangioma (arrow) in the left hepatic lobe. **2.3** Ferucarbotran-enhanced T2*-weighted GRE image shows ghosting artifacts (arrow) arising from the aorta, which obscure the hemangioma in the left hepatic lobe.

Figure 3:
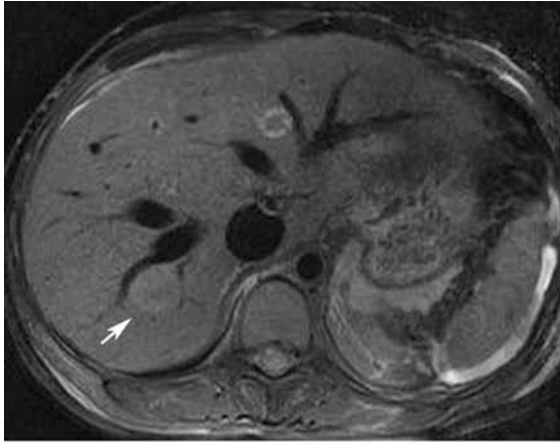
3.1
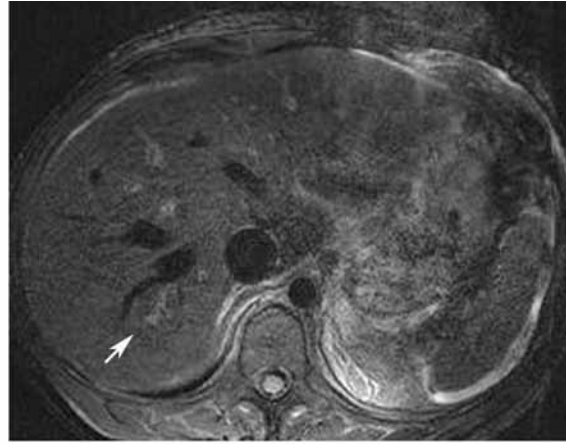
3.2
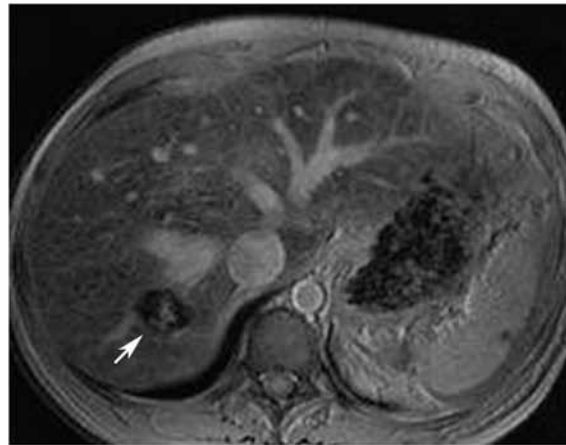
3.3

Hepatic adenoma in a patient with cardiomyopathy.

3.1 Unenhanced T2-weighted FSE image shows a slightly hyperintense lesion (arrow) in segment VII. **3.2** Ferucarbotran-enhanced T2-weighted FSE image shows an isointense lesion (arrow) with a central focus of high signal intensity. **3.3** Ferucarbotran-enhanced T2*-weighted GRE image shows a lesion with low signal intensity a central focus of high signal intensity (arrow). This low signal intensity of the lesion was found typical for adenoma and can be used for the differentiation from FNH.
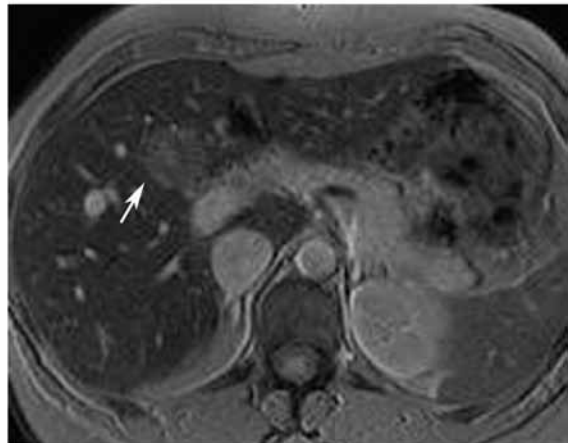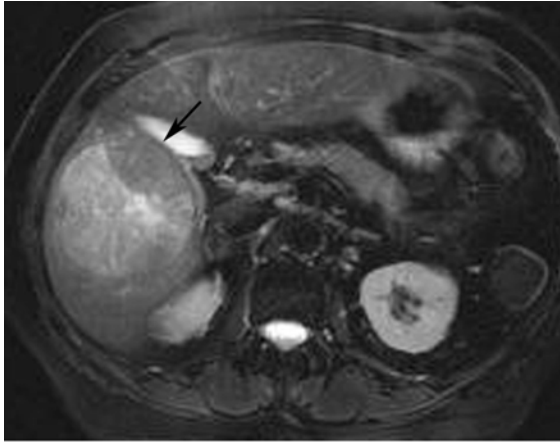
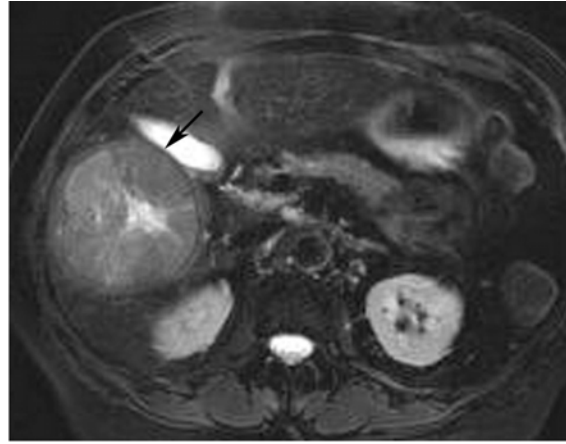**Figure 4:**
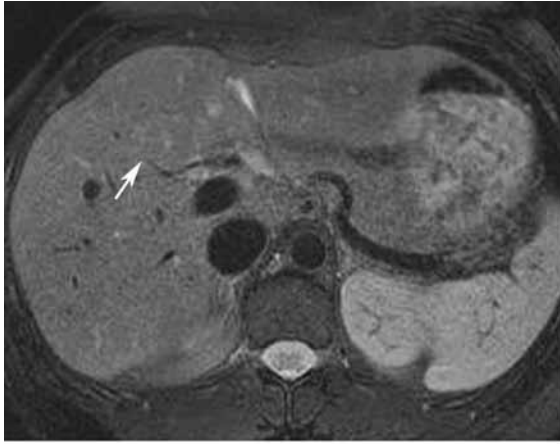
4.1
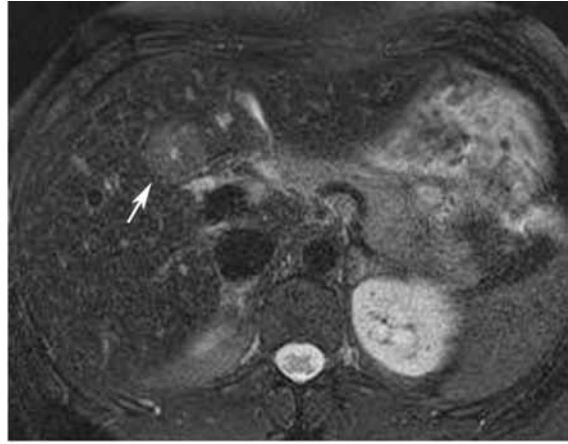
4.2

4.3

Focal nodular hyperplasia.

4.1 Unenhanced T2-weighted FSE image shows a focal iso-intense lesion (arrow) in segment IV. **4.2** Ferucarbotran-enhanced T2-weighted FSE, and **4.3** Ferucarbotran-enhanced T2*-weighted GRE images show a slightly hyperintense focal lesion (arrow) in segment IV. The central scar is best seen as a hyperintense focus in **4.2**.
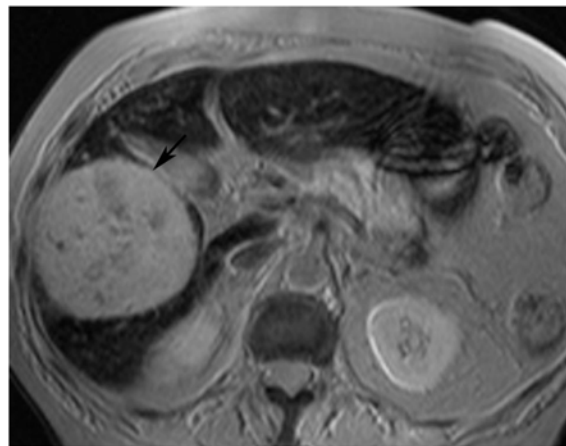
Figure 5:

5.1

5.2

5.3

Hepatocellular carcinoma with mosaic pattern and peripheral capsule.
5.1 Unenhanced-, and **5.2** Ferucarbotran-enhanced T2-weighted FSE images show a well-marginated round mass (arrow) with mosaic pattern and hypointense capsule in right hepatic lobe. Some portion of the mass shows signal loss after ferucarbotran administration. **5.3** Ferucarbotran-enhanced T2*-weighted GRE image exhibits a hyperintense mass (arrow) with no definite mosaic pattern nor peripheral capsule; however, the contrast between the lesion and the adjacent liver parenchyma is best seen in **5.3**.
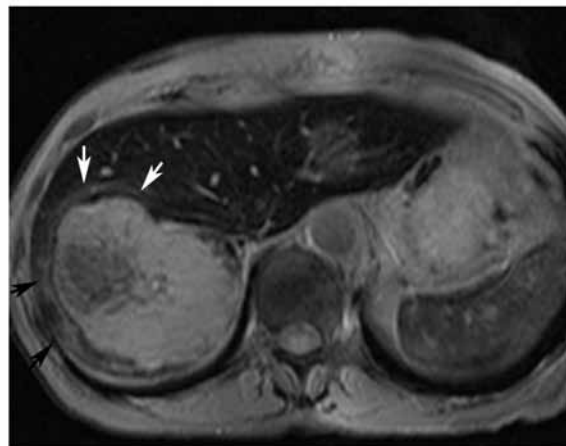
Figure 6:
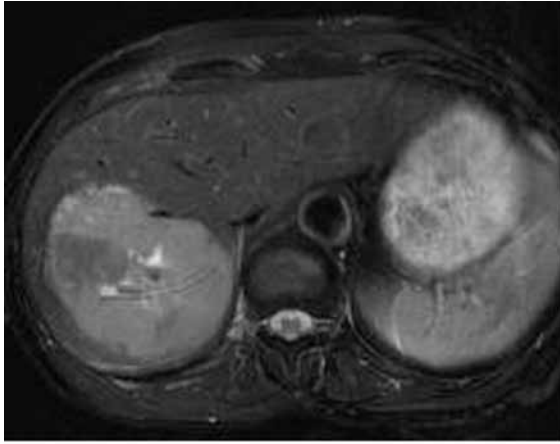
6.1
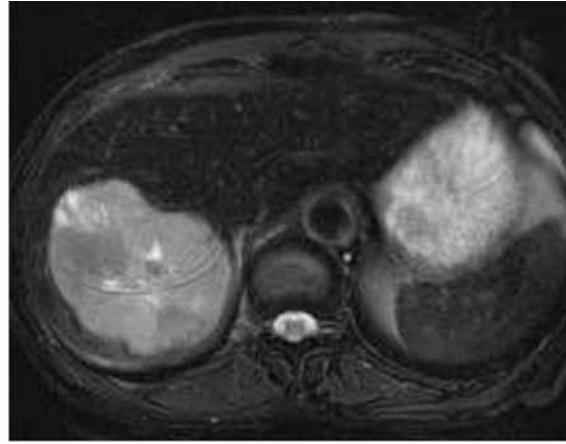
6.2

6.3

Metastasis from a colorectal carcinoma with hyperintense rim outside the tumor.

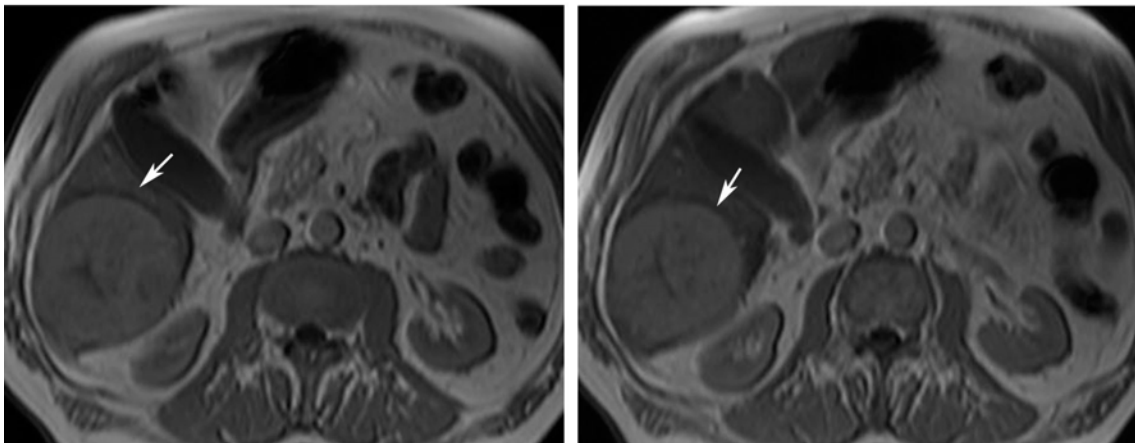**6.1** Unenhanced-, **6.2** Ferucarbotran-enhanced T2-weighted FSE, and **6.3** Ferucarbotran-enhanced T2*-weighted GRE images show a well-marginated hyperintense mass with hyperintense foci mimicking a central scar in the right hepatic lobe. The mass lesion is depicted with increased tumor-to-liver contrast after ferucarbotran administration. The hyperintense rim (arrows) outside the tumor is best seen in **6.3**.

Figure 7:
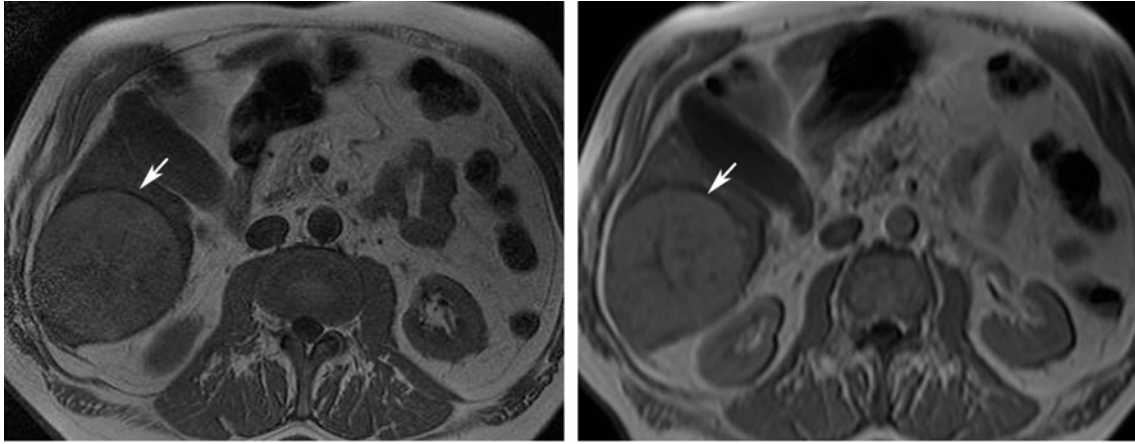
Hepatocellular carcinoma on ferucarbotran enhanced dynamic T1-weighted 2D-GRE images.

7.1 Pre-contrast; **7.2** 20 seconds; **7.3** 50 seconds; and **7.4** 120 seconds. A well demarcated, round, slightly hyperintense mass (arrow) in the right hepatic lobe without significant signal intensity change at before and after contrast agent injection is seen.

Figure 8:

8.1

8.2

8.3

8.4

Metastasis on ferucarbotran enhanced dynamic T1-weighted 2D-GRE images.

8.1 Pre-contrast; **8.2** 20 seconds; **8.3** 50 seconds; and **8.4** 120 seconds. A well demarcated and lobulated, hypointense mass (arrow) in right hepatic lobe with ring enhancement (**8.3 and 8.4**) outside the tumor margin can be delineated.
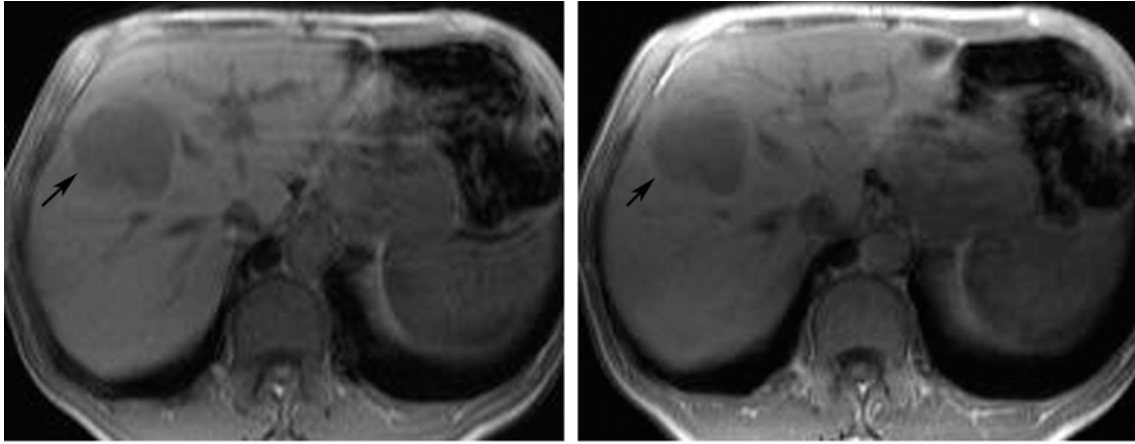
Figure 9:

9.1

9.2
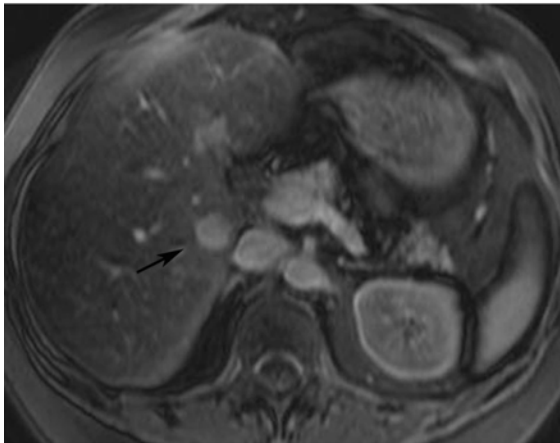
9.3

9.4

Adenoma on ferucarbotran enhanced dynamic T1-weighted 3D-GRE VIBE images.
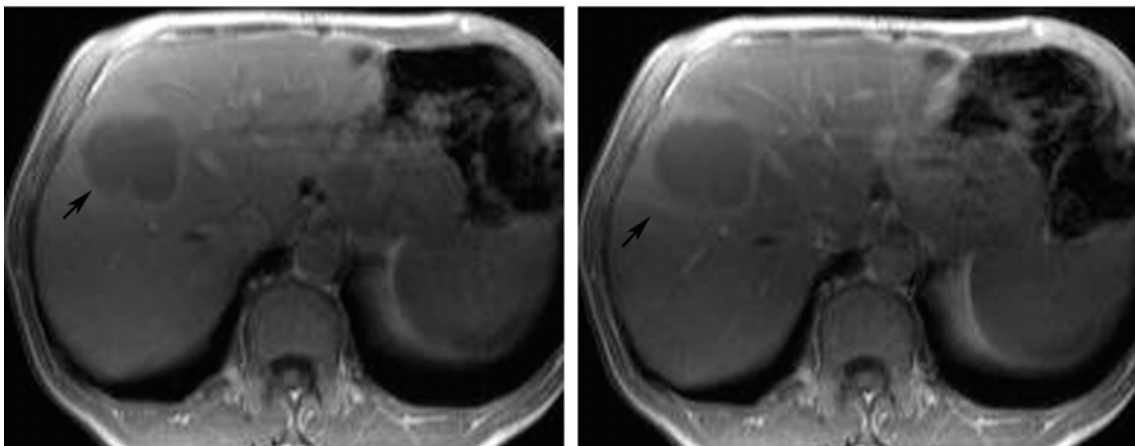**9.1** Pre-contrast; **9.2** 20 seconds; **9.3** 50 seconds; and **9.4** 120 seconds. A well-demarcated, persistent hyperintense mass (arrow) adjacent to the inferior vena cava before and after contrast agent injection can be noted.

Figure 10:

10.1

10.2
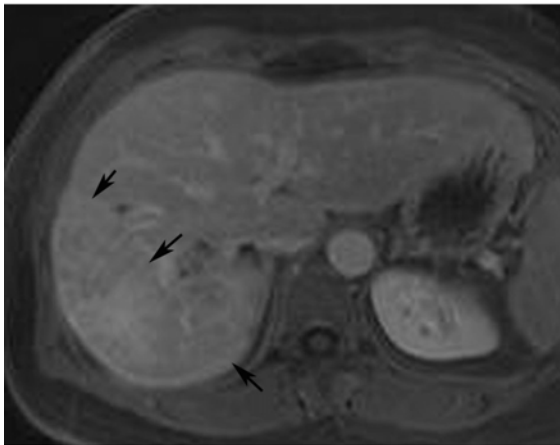
10.3
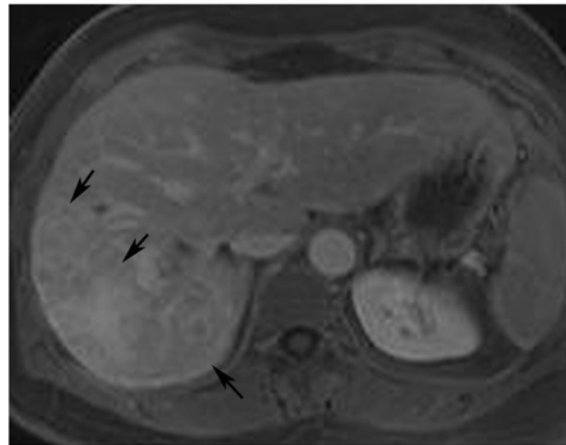
10.4

Focal nodular hyperplasia on ferucarbotran enhanced dynamic T1-weighted 3D-GRE VIBE images.

10.1 Pre-contrast; **10.2** 20 seconds; **10.3** 50 seconds; and **10.4** 120 seconds. A conglomerated mass with central scar (arrows) in right hepatic lobe can be seen. After contrast agent injection the lesion shows isointensity to the liver parenchyma and the central scar shows gradual contrast enhancement.
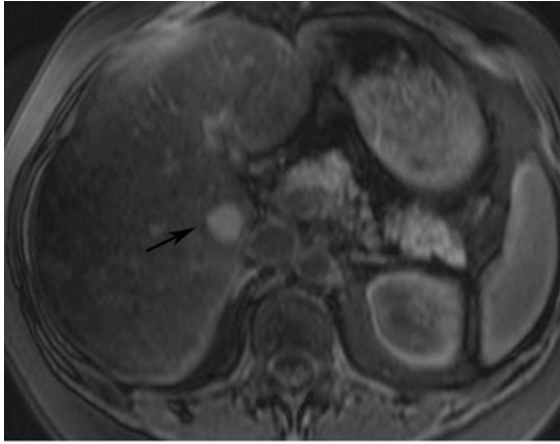
Figure 11:

11.1
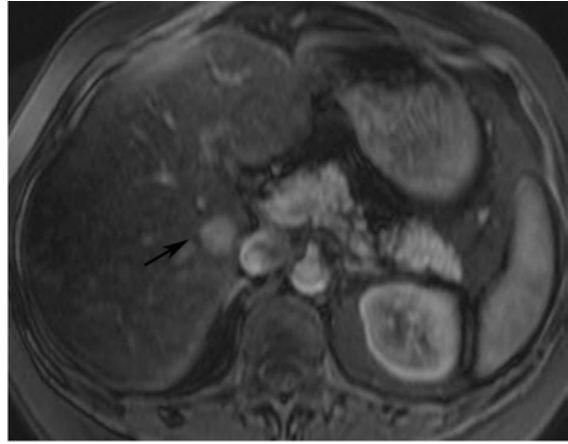

11.2
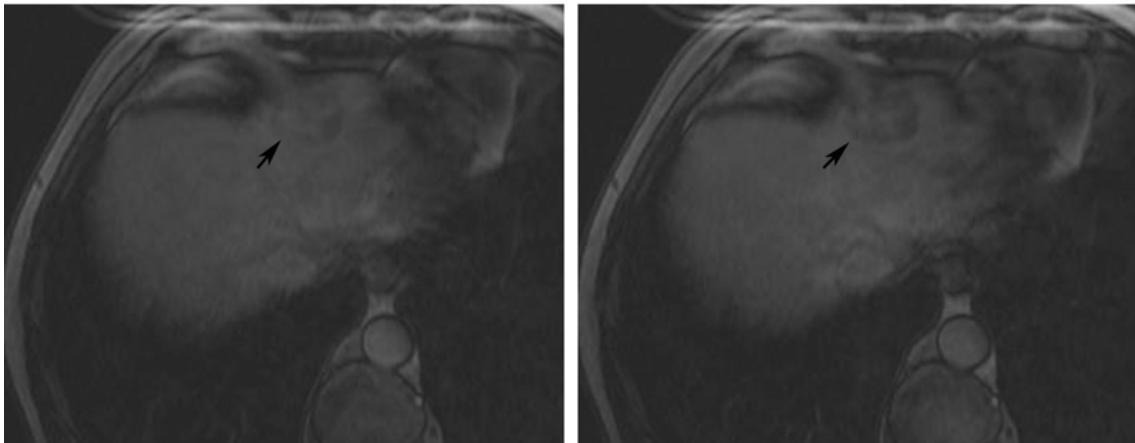
11.3

11.4

Hemangioma on ferucarbotran enhanced dynamic T1-weighted 3D-GRE VIBE images. **11.1** Pre-contrast; **11.2** 20 seconds; **11.3** 50 seconds; and **11.4** 120 seconds. A well-demarcated mass (arrow) in left hepatic lobe can be delineated. After contrast agent injection the lesion shows nodular, peripheral enhancement in the arterial phase and the typical fill-in enhancement over time.
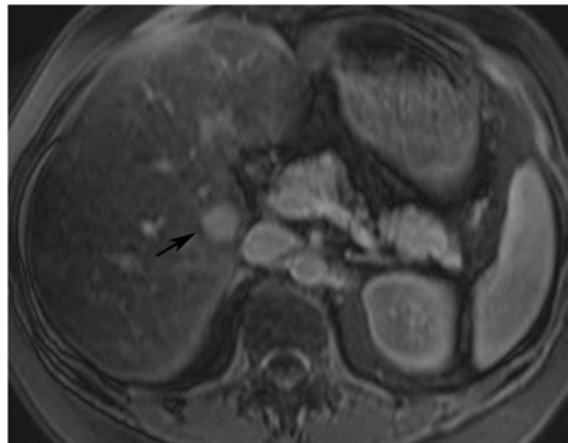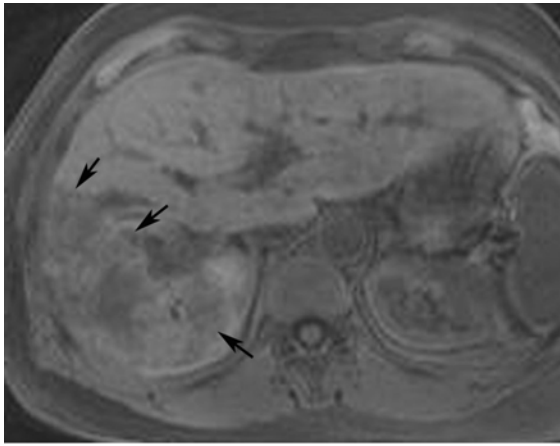
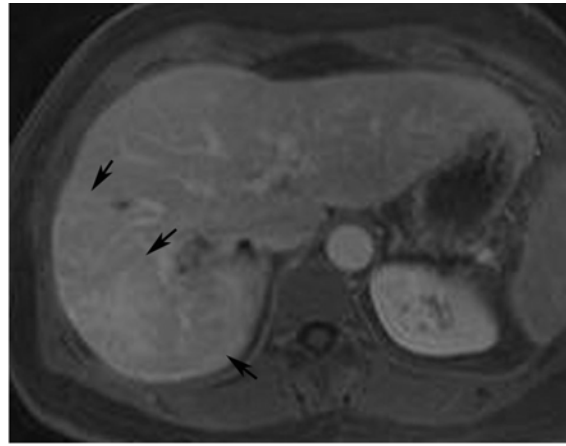**Figure 12:**

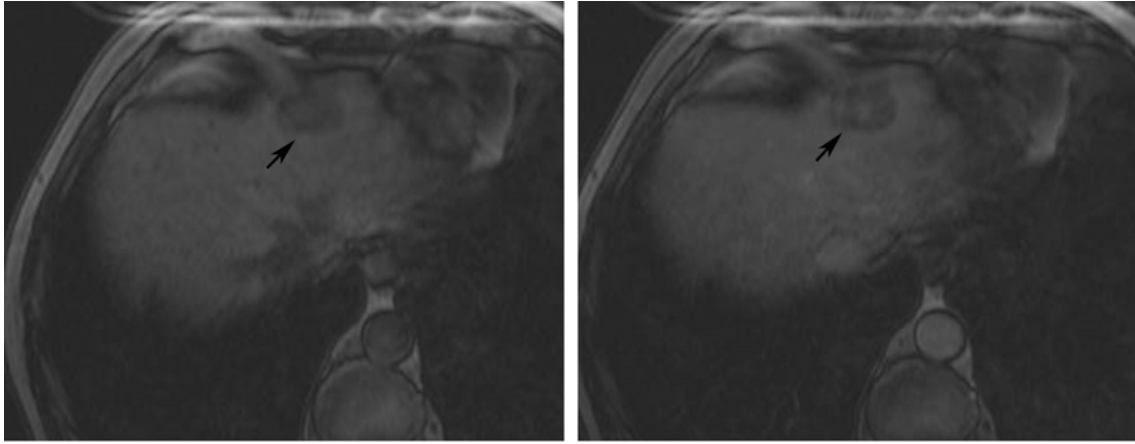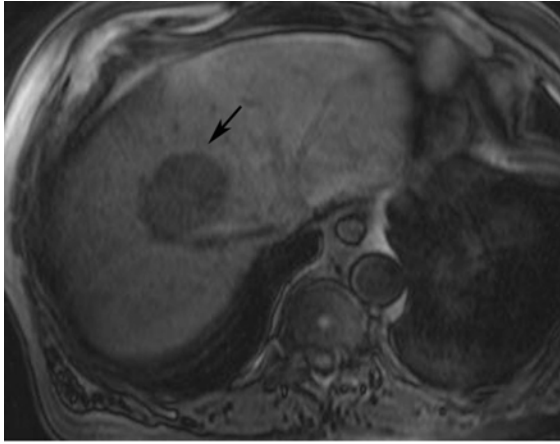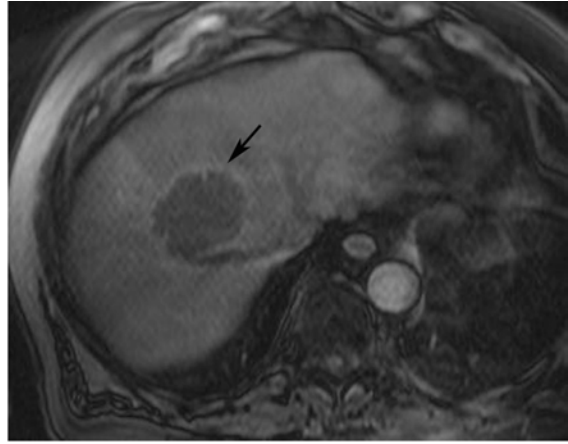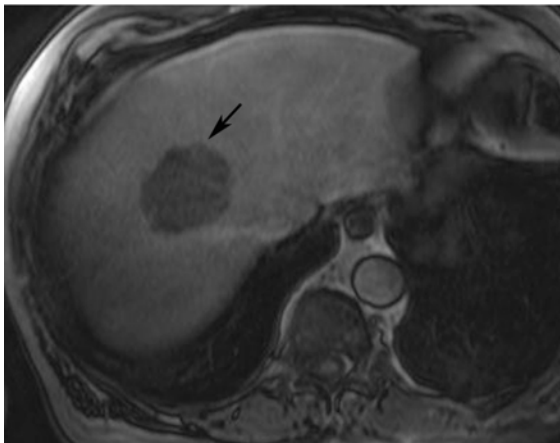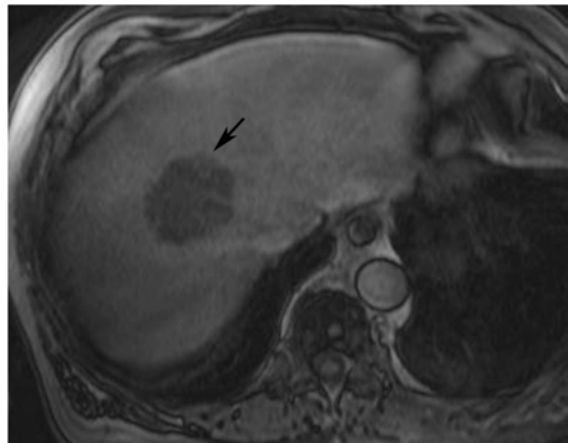Hepatocelluar carcinoma on ferucarbotran enhanced dynamic T1-weighted 3D-GRE VIBE images.

12.1 Pre-contrast; **12.2** 20 seconds; **12.3** 50 seconds; and **12.4** 120 seconds. A well-demarcated and slightly lobulated, hypointense lesion (arrow) in the right hepatic lobe can be seen. The lesion shows ring enhancement in outside the tumor margin.

5. DISCUSSION

The characterization of focal liver lesions as well as their detection is an important issue in liver imaging with major impact on further patient treatment and prognosis. The use of extracellular gadolinium chelate contrast agents has improved the capability for lesion characterization in liver MR imaging based on tumor vascularity and diffusion of contrast agent into the extracellular space (6,49,55). Extracellular gadolinium chelates are primarily useful for tissue characterization of focal liver lesions with evaluation of the enhancement pattern using dynamic MR imaging. However, the detection rate is considered being not sufficiently high by many authors (15,18,20,37,47,59).

SPIO agents are primarily known to improve the detection of lesions with increased tumor-to-tissue contrast (1,11,28,36) and considered to be useful in preoperative liver MR imaging (1,4,10,46,48). In SPIO-enhanced MRI the differentiation between benign and malignant focal liver lesions is also possible on the basis of its cellular composition (RES cells in normal liver parenchyma and tumor) and function (2,3,36). Therefore, when the diagnostic efficacy of SPIO-enhanced liver MRI for the characterization of focal lesions is as sufficiently high as gadolinium chelates enhancement, it can be used as a useful diagnostic method with a cost-benefit and time-saving for the pretreatment or preoperative evaluation and follow-up imaging in patients with malignant liver lesions.

5.1 Ferucarbotran-enhanced T2-/T2*- weighted Imaging Sequences

5.1.1 Characterization of Focal Liver Lesions

SPIO agents are mainly used as negative contrast agents in the accumulation phase on T2/T2*-w sequences with decreased SI of normal liver parenchyma and nearly unchanged SI of focal lesions without reticuloendothelial cells. Typically, malignant liver lesions devoid of Kupffer's cells, such as metastases or HCC appear as hyperintense lesions without significant SI loss against the dark background of the liver on SPIO-enhanced MRI. In contrast, tumors with Kupffer's cells, such as FNHs, adenomas and regenerative nodules or with a relevant blood pool, such as hemangiomas show a decrease in SI after SPIO administration. (4,11,36,55).

PSIL

The quantification of the PSIL after SPIO application is considered to be different between noncystic benign and malignant lesions and might be used for the differentiation between benign and malignant lesions in SPIO-enhanced liver MR imaging (4,11,36,55).

Vogl et al (55) reported a sensitivity of 88% and specificity of 89% with a threshold PSIL of 10% for distinguishing benign from malignant liver lesions on ferumoxide-enhanced proton-density-w MR images. In the present study, we evaluated the PSIL with a standard T2-w FSE sequence. The PSIL of noncystic benign lesions was statistically significantly higher than that of malignant lesions. We could obtain a sensitivity of 97.8% and specificity of 92.9% with a threshold PSIL of 25% for

distinguishing benign from malignant liver lesions. With a threshold PSIL of 20% or 30% results were not dramatically worsened, so that there is still some safety buffer left. According to the results of previous and the present studies, therefore, we suggest that the differentiation between benign and malignant focal liver lesions is feasible with help of PSIL and should be performed in all cases, in which characterization of lesion is doubtful on visual evaluation. However, as a prerequisite for performing PSIL calculations the same T2-w FSE sequence has to be performed pre- and post SPIO-application.

Characterization of each lesion type by means of PSIL is considered problematic in the literature, because the PSIL can vary with different imaging sequences and has shown overlap between the several lesion types in the existing literature. For example, the mean PSIL have been reported as 8.8%, 41.0% ± 18.3 and 42% ± 9 in FNH, 32.4% ± 6.9 and 74% in adenomas, and 11.2% ± 6.3, 21% ± 16 and 56% (range in 30 − 70%) in hemangiomas. Moreover, previous studies also reported an overlap between the PSIL of some benign lesions with that of well-differentiated HCC (4,11,14,55).

As shown in Graph 3 we also found variable and overlapping PSIL; however, mainly in malignant lesions. In our study the PSIL was not overlapped among adenomas, FNHs and hemangiomas, and the PSIL of adenomas was significantly higher than the PSIL of FNHs, and the PSIL of FNHs was significantly higher than that of hemangiomas. Therefore, in contrast to previous studies, we also suggest that it may be possible to differentiate each benign lesion type by means of PSIL.

Differentiation between FNH and adenomas

Adenomas showed dark signal intensity on CE-T2*-w GRE images, which resulted in superior lesion conspicuity and lesion detectability in this sequence in contrast to CE-T2-w FSE images. As previously reported by Vogl et al. (55), some adenomas showed central foci of high signal intensity within a mainly low signal intensity lesion on CE-T2*-w GRE images. In previous reports (36,55) as well as in the present study, FNH showed never hypointensity as compared to surrounding liver parenchyma on SPIO-enhanced MR images. Therefore, the finding of dark signal intensity lesion with central high signal intensity foci on CE-T2*-w GRE images can be useful in the diagnosis of adenoma in SPIO-enhanced MRI.

Diagnosis of Hemangioma

Hemangiomas showed variable SI from hypo- to highly hyperintensity with variable SNR and CNR on CE-T2-w FSE and CE-T2*-w GRE images. Therefore, with both sequences the diagnosis of hemangioma and differentiation from other benign or malignant lesions may be difficult, and heavily T2-w FSE images as well as dynamic contrast-agent behavior is needed for the definite diagnosis of hemangioma. The reason for the variable imaging findings after SPIO application might be the variable pathomorphology of hemangiomas. To our mind hemangiomas with few parenchyma (and few Kupffer cells) and large intravascular space show a different behavior than hemangiomas with more parenchyma and more Kupffer cells.

Differentiation between HCC and Metastases

Both HCC and metastasis are presented with hyperintensity with no statistically significant difference in the SNR and CNR between two lesion types on both NCE- and CE- imaging sequences, except for the CNR on CE-T2-w image. The PSIL were also not statistically significantly different between two lesion types. Therefore, differentiation between HCC and metastases may be impossible only with SI evaluation of the lesions. It has been pointed out in various studies that in everyday clinical practice it is necessary to use visual criteria of morphologic features such as scar, capsule, hemorrhage, background cirrhosis in conjunction with quantitative criteria such as CNR and PSIL to achieve a correct diagnosis (6,36).

Differentiation between Malignant and Coexisting Benign Lesions

Another difficulty in SPIO-enhanced MR imaging is differentiating malignant lesions with a cystic appearance from incidental coexisting benign lesions, such as hepatic cysts and hemangiomas. These lesions may appear highly hyperintense against the black background of the liver, and small cysts or hemangiomas less than 10 mm may be a substantial source of false-positive finding on SPIO-enhanced MR imaging (4,5,24,35). At present, NCE-heavily T2-w SE sequences are considered helpful for the differentiation of hemangiomas and cysts from metastases (30,31,35). We also obtained the result that on NCE-T2-w FSE images the CNR of cysts and hemangiomas were statistically significantly higher than those of HCC or metastases. Moreover, we found that on CE-T2*-w GRE images the SNR and CNR of cysts were significantly lower than those of HCC or metastases.

5.1.2 Comparison of the Diagnostic Efficacy between T2-weighted FSE and T2*-w GRE Sequences in Ferucarbotran-enhanced Liver MRI

We evaluated and compared the efficacy of T2-w FSE and T2*-w GRE images in ferucarbotran-enhanced liver MRI by means of qualitative as well as quantitative analysis, because the optimum imaging sequence has been one of the subjects of debate (1,24,40,51,53,58)..

Overall Image Quality and Imaging Artifacts

Overall image quality was superior on CE-T2*-w GRE images over CE-T2-w FSE images, which was mainly caused by the high number of examinations (48.5%) with motion artifacts on T2-w FSE images. Especially in patients with a large amount of ascites the motion artifacts in T2-w FSE sequences were so severe that they interfered with image interpretation and obscured focal lesions. Artifacts arising on T2*-w GRE images were mainly ghosting artifacts. However, their number was with 11.8% significantly lower than artifacts in T2-w FSE images. Moreover, the ghost artifacts did not affect image quality or image interpretation as much as motion artifacts in the T2-w images. Just in one case of hemangioma within our study group the lesion was obscured by a ghost artifact from the aorta on the CE-T2*-w GRE sequence. However, image degradation from metallic artifacts was more severe on T2*-w GRE images due to the sensitivity to susceptibility (1,5,12).

Lesion and Vessel Conspicuity

Kanematsu et al. (24) reported that on ferumoxide-enhanced T2*-w GRE images using 150/10 (TR msec/TE msec) the CNR of malignant lesions was lower than on T2-w FSE images and was almost the same in nonsolid benign lesions. Therefore, they suggested that the differentiation between nonsolid benign and solid malignant lesions might be difficult on ferumoxide-enhanced T2*-w GRE images.

In our study, however, lesion conspicuity of malignant lesions was superior with a high CNR on CE-T2*-w GRE images with 117/10/30° (TR msec/TE msec/flip angle) in contrast to CE- T2-w FSE images. Especially in HCC, the CNR was significantly higher on CE-T2*-w GRE images than on CE- T2-w FSE images, which might be the main reason for the superior lesion conspicuity and lesion detectability. In hepatic cysts the lower lesion conspicuity with only slight hyperintensity on CE-T2*-w GRE images was helpful to differentiate them from markedly hyperintense malignant lesions. Therefore, we suggest that T2*-w GRE sequence are especially helpful for lesion detection; however they can be also helpful for the differentiation between hepatic cysts and malignant lesions.

Adenomas showed dark signal intensity on CE-T2*-w GRE images, which resulted in superior lesion conspicuity and lesion detectability in this sequence in contrast to CE-T2-w FSE images.

It has been reported that on T2*-w GRE images vessel are depicted hyperintense with high vessel-to-liver CNR, whereas on T2-w SE or FSE uneven signal intensity is noted. Therefore, T2*-w GRE are considered to be more useful for preoperative segmental analysis of focal liver lesions than T2-w SE or FSE images (53). We could also

demonstrate superior vessel conspicuity on T2*-w GRE images.

Evaluation of Morphological Feature and Secondary Findings of the Tumor

We investigated the efficacy of T2-w FSE and T2*-w GRE sequences for the evaluation of morphological features of focal lesions, such as mosaic pattern, capsule, scar and portal vein thrombosis. There was no significant difference in the efficacy for the evaluation of these morphological features between the two imaging sequences. Only in the evaluation of mosaic pattern a tendency of superiority on T2-w FSE images was noted. The hyperintense ring at the rim of a malignant tumor might be a helpful finding for characterization of focal liver lesions in SPIO-enhanced MR imaging (19,32,41). In our study this finding was noted easier on CE-T2*-w GRE than on CE-T2-w FSE sequences without statistical significance.

5.2 Ferucarbotran-enhanced T1-weighted Dynamic MR Imaging

SPIO agents can also be used as positive contrast agents due to T1 shortening at low concentrations. Several studies could show an improved characterization of focal liver lesions on T1-w images in the accumulation phase (13,35,44).

Ferucarbotran is a bolus-injectable SPIO agent without cardiovascular side effect (1,17,56). The characterization of focal liver lesions by means of ferucarbotran-enhanced dynamic MR imaging has been reported and characteristic findings have been demonstrated in a limited number of cases (34,39,41,54).

We performed ferucarbotran-enhanced T1-w dynamic MR imaging using two different GRE sequences (2D-GRE and 3D-GRE VIBE) and evaluated the change in SNR and CNR of normal liver tissue, vascular structures and focal liver lesions on each sequences. We could find out differences in change of SNR and CNR and enhancement patterns of the liver, vascular structures and focal lesions between the two sequences.

5.2.1 Evaluation of Enhancement Pattern in Liver and Vascular Structures

All vascular structures (aorta, portal vein and IVC) showed early increase in SNR at 20 seconds after injection on both sequences, however the increase was more pronounced in the 3D-GRE images. The SNR of the liver showed also an early increase at 20 seconds after injection. The resulting CNR between all vascular structures and the liver parenchyma showed negative values at 20 and 50 seconds after injection for 2D-GRE images, which means that vascular structures were hypointense in comparison to the liver parenchyma and could mimic small focal liver lesions. In contrast, on 3D-GRE VIBE images the vascular structures showed positive CNR at all time points after injection. In addition, the change in SNR and CNR of the aorta on 3D-GRE VIBE images was similar to that known from gadolinium chelates with an early rapid increase followed by a slight decrease with persistent positive enhancement (27). These findings suggest that the 3D-GRE VIBE sequence is more useful in comparison to a 2D-GRE sequence for the evaluation of the vascular structures and for the differentiation between vascular structure and small focal lesion.

5.2.2 Evaluation of Enhancement Pattern in Focal Liver Lesions

Tumor Vascularity

Vogl et al. (54) reported a rapid decrease in SI of hypervascular tumors such as FNH, hemangioma and HCC between 22 and 44 seconds after injection of ferucarbotran on T2-w GRE sequence. These lesion types showed a rapid increase in SI on T1-w GRE sequences, whereas metastasis did not demonstrate significant change of SI on T1-w GRE and T2-w GRE sequences (34,39,41,54). Therefore the authors suggested that dynamic imaging of the perfusion phase with SPIO might be used to evaluate tumor vascularity.

With regard to lesion vascularity our study showed different findings as compared to previous reports. We could also observe differences in the enhancement pattern of different liver lesions between 2D-GRE and 3D-GRE VIBE sequences.

Both HCC and metastasis showed similar changes of SNR on 2D-GRE sequences with an increase at 20 seconds, which was not noticed on 3D-GRE VIBE dynamic sequences. A persistent negative mean CNR was seen in both lesions and in both sequences at all time points. The expected strong enhancement of HCC with positive contrast at least 20 seconds after injection could not be identified, suggesting that the evaluation of tumor vascularity in malignant liver lesions for differentiation between hypervascular HCC and hypovascular metastases with ferucarbotran-enhanced T1-w dynamic GRE imaging, either with 2D or 3D technique, is difficult or impossible.

With regard to benign hypervascularized liver lesions two different groups have to be

considered, on the one hand hemagioma on the other adenoma and FNH.

In our study all hemangiomas (n=6) showed centripetal fill-in enhancement with an early increase in SI at 20 and/or 50 seconds. Moreover, two hemangiomas showed the typical nodular enhancement in 3D-GRE VIBE images. These results are comparable to previous studies (34,39,41).

In FNH and adenoma, however, hypervascularity could not be demonstrated with ferucarbotran-enhanced dynamic MRI in our series. All FNHs showed more or less isointensity with a CNR around zero at all time points. All adenomas showed no early increase in SNR and CNR and showed relatively consistent values after ferucarbotran-enhanced T1-w images in contrast to gadolinium-enhanced dynamic MRI.

Therefore we suggest that ferucarbotran-enhanced dynamic T1-w GRE MRI has a different enhancement mechanism and is not giving the same information for the evaluation of tumor vascularity as gadolinium chelates.

Characteristic Findings in Benign Liver Lesions

All hemangiomas (n=6) showed centripetal fill-in enhancement pattern on both 2D and 3D techniques. Moreover, two hemangiomas showed the typical nodular enhancement in 3D-GRE VIBE images.

We could also observe specific findings in a limited number of FNH (n=3) and adenoma (n=3) at 3D-GRE VIBE images. All FNHs showed more or less isointensity at all time points. In 2/3 cases an internal scar could be detected on dynamic images with gradual enhancement comparable with gadolinium-enhanced dynamic MRI.

Adenoma showed the highest SNR and CNR at precontrast and contrast enhanced

dynamic images in our study. The high SI on precontrast T1-w images can be explained by a high glycogen content of the cells (2,3). Consistent high SI without significant change on ferucarbotran-enhanced T1-w GRE dynamic imaging may be used as a specific finding in the diagnosis of adenoma in comparison to malignant lesions and FNHs, which presented hypointense respectively isointense in our series at all post-contrast imaging time points.

Cysts showed the lowest SNR and CNR values without significant enhancement, which is also a typical finding on gadolinium-enhanced dynamic MRI.

Differentiation between Benign and Malignant Focal Lesions

One possibility for the differentiation of benign from malignant lesions, especially in metastases, is presence of ring enhancement in malignant lesions adjacent to the tumor on SPIO-enhanced static and dynamic T1-w GRE MRI, which showed ring enhancement of liver metastases significantly more frequently (80%) than $T2^*$-w GRE (36%) (19,32,34,39,41). In our study a ring enhancement pattern was demonstrated in only two of four metastases on 2D-GRE images and none of 10 metastases on 3D-GRE VIBE images. The discrepancy of the rates between previous reports and our study may be explained with the different time points for the dynamic studies. The ring enhancement pattern reported in the literature was demonstrated mainly at late perfusion (> 120 sec) and accumulation phases (19,32,39). However, we performed early dynamic studies only up to 120 seconds after injection. This difference might be the explanation for a less frequently demonstrated ring enhancement pattern in metastases in our study.

On 3D-GRE VIBE dynamic sequences benign solid lesions including hemangiomas

showed isointensity or slight hyperintensity at all time points whereas most of malignant lesions showed marked hypointensity. This finding can be used for the differentiation between benign and malignant lesions in the early dynamic phase. Further delayed images (over 120 seconds after injection) may be helpful to differentiate malignant lesions from slowly and gradually enhancing hemangioma.

5.2.3 Advantages of 3D-GRE VIBE sequences over 2D-GRE in ferucarbotran-enhanced dynamic T1-w liver MR Imaging

3D-GRE VIBE may be more useful for the evaluation of the vascular structure and for the differentiation between vascular structures and small focal liver lesion 50 seconds after injection. Moreover, with 3D-GRE VIBE the differentiation between benign and malignant lesions and specific diagnosis of benign lesions (cyst, adenoma, hemangioma, FNH) may be possible.

In addition, 3D imaging has potential advantages over 2D imaging. In comparison with traditional 2D GRE sequences, 3D GRE VIBE sequences have the capacity to provide thinner sections, no gaps, fat saturation, higher SNR, and comparable image contrast in the same breath-hold time frame. Therefore, with 3D GRE VIBE imaging, the pitfalls of intersection gaps and partial volume artifacts associated with 2D imaging can be avoided, and fat saturation improves CNR and reduces the potential degradation of image quality resulting from motion-related artifacts. Other advantages include the opportunity to reformat images in any plane without loss of image resolution. The sequence also differs by including a decreased flip angle to improve contrast in

abdominal imaging (27,42).

5.3 Study limitation

A number of limitations are present in this study.

First, the exact comparison between T2-w FSE and T2*-w GRE sequences with regard to the ferucarbotran effect and the PSIL was impossible, because our routine protocol for ferucarbotran-enhanced liver MRI contained no NCE-T2*-w GRE sequence, which is considered unnecessary precontrast due to the low soft tissue contrast.

Second, pathologic correlation was not available in every case in our study and that an exact lesion tracking was not possible. Therefore the results of lesion detection in comparison of T2-w FSE and T2*-w GRE sequences might have a systemic mistake.

At last, the number of patients, especially with benign liver lesions was small. Moreover, the selection of only one lesion per patient even in patients with multiple lesions can be criticized. However, this was mainly done since in our experience the enhancement pattern of the same lesion type within the same patient was constant. By evaluation of more than one lesion per patient the number of evaluated lesions would have been far higher suggesting a higher statistical confidence than would be realistic.

5.4 Conclusion

Solid benign lesions show SPIO uptake with a significant signal loss in a T2-w FSE

sequence in contrast to malignant lesions. When a threshold of 25% is used, PSIL is an accurate tool for the characterization of benign and malignant lesions. For the detection of malignant lesions, the additional use of a CE-T2*-w GRE sequence is helpful due to the significantly higher CNR, a superior lesion conspicuity and better image quality in comparison to a CE-T2-w FSE sequence.

Early dynamic ferucarbotran-enhanced MRI with T1-w sequences is feasible. However, neither T1-w 3D-GRE VIBE nor T1-w 2D-GRE sequences did provide the same information known from dynamic gadolinium-enhanced MRI. For the evaluation of the liver vasculature the 3D-GRE VIBE sequence exhibits advantages, since it better resembles the vascular enhancement pattern known from gadolinium. The observed enhancement pattern of focal liver lesions in ferucarbotran-enhanced 3D-GRE VIBE seemed more specific than in 2D-GRE imaging, so that differentiation between malignant and benign lesions might be possible in the 3D-GRE VIBE sequence.

In clinical implication of ferucarbotran-enhanced liver MRI, the differentiation between benign and malignant lesions can be possible with PSIL at T2-w FSE imaging sequence. The differentiation between the benign lesions (adenoma, FNH and hemangioma) may be possible with the evaluation of enhancement pattern at dynamic T1-w GRE sequences. Unless using the visual criteria of morphologic features such as scar, capsule, hemorrhage, background cirrhosis, neither the PSIL at T2-w FSE nor the enhancement pattern at dynamic T1-w GRE sequences can help to differentiate the malignant lesions (HCC, metastasis and CCC).

6. SUMMARY

Superparamagnetic iron oxides (SPIO)-enhanced liver MRI is considered a useful preoperative diagnostic method with high sensitivity and specificity for the detection of focal liver lesions. With SPIO-enhanced MRI the differentiation between benign and malignant focal liver lesions is also possible on the basis of its cellular composition (RES cells in normal liver parenchyma and tumor) and function.

In earlier clinical trials the effects of SPIO particles were evaluated almost exclusively at T2-weighted (w) fast-spin echo (FSE) and T2*-w gradient echo (GRE) sequences because of main T2- or T2*- shortening effect of the SPIO particles.

Ferucarbotran is a bolus-injectable SPIO agent without cardiovascular side effect. Dynamic T1-w perfusion MRI following bolus injection of ferucarbotran might provide information about the vascularity of solid liver lesions. The characterization of focal liver lesions by means of ferucarbotran-enhanced dynamic MR imaging has been reported and characteristic findings have been demonstrated on a limited number of cases.

The first purpose of our study was to evaluate the efficacy of SPIO agent ferucarbotran in T2-w FSE and T2*-w GRE sequences for the characterization of focal liver lesions. The second aim was to evaluate the enhancement pattern of ferucarbotran-enhanced early dynamic MR imaging with 2D-GRE and 3D-GRE VIBE sequences for the characterization of focal liver lesions.

On a 1.5 T MR-system noncontrast-enhanced (NCE) and contrast-enhanced (CE) T2-w

FSE images and CE- T2*-w GRE images 10 minutes after i.v.-injection of 1.4 ml ferucarbotran were obtained in 68 patients.

On a 1.5 T MR system T1-w dynamic images were obtained with 2D-GRE sequences in 23 patients and 3D-GRE VIBE sequence in 37 patients.

The final diagnoses of the 68 patients, in whom T2-w FSE/ T2*-w GRE sequences were performed, included hepatocellular carcinomas (HCC, n=29), metastases (n=15), cholangiocellular carcinomas (CCC, n=2), hemangiomas (n=6), adenomas (n=5), focal nodular hyperplasias (FNH, n=3) and cysts (n=8).

The final diagnoses of the 60 patients, in whom T1-w early dynamic MR imaging was performed, included HCC (n=25), metastasis (n=14), CCC (n=2), hemangiomas (n=6), adenomas (n=3), FNH (n=3) and cysts (n=7).

On T2-w FSE/ T2*-w GRE images the signal-to-noise ratio (SNR) and contrast-to-noise ratio (CNR) based on signal intensity measurements in focal lesions and liver parenchyma were calculated for all sequences. The percentage signal intensity loss (PSIL) of focal lesions from NCE- to CE- was calculated for the T2-w FSE sequence. Qualitative analysis was performed for the image quality and lesion conspicuity at CE-T2-w FSE and CE-T2*-w GRE sequences.

In T1-w early dynamic MR imaging SI measurements in the liver parenchyma, the hepatic vasculature and in focal lesions were performed precontrast and 20, 50 and 120 seconds after bolus-injection of ferucarbotran to calculate the SNR and CNR.

The mean SNR of solid benign lesions showed a decrease from 34.1 to 21.0 (p<0.05). In malignant lesions, the mean SNR showed only a minor decrease from 33.3 to 32.5. The mean CNR of the malignant lesions was the highest in the CE-T2*-w sequence as

compared to the post- and the pre-contrast T2-w FSE sequence (29.9 vs. 22.7 (p<0.01) vs. 12.8 SI (p<0.01)). With a threshold PSIL of 25 %, the sensitivity and specificity for the characterization of malignant lesions was 97.8% respectively 92.9% in ferucarbotran-enhanced T2-w FSE. There was no overlap between the PSIL of adenoma and FNH. CE-T2*-w GRE images showed a superior image quality and lesion conspicuity (p < .05) as compared to the CE-T2-w FSE sequence.

With early dynamic ferucarbotran-enhanced MRI hypervascularity could not be shown in typically hypervascularizied lesions such as HCCs, adenomas or FNHs. In hemangiomas fill-in enhancement could be observed in all cases. In the 3D-GRE sequence mean CNR for solid benign lesions was around zero (FNH) or markedly positive (adenoma), whereas mean CNR for malignant lesions was negative at all time points.

In conclusion, solid benign lesions show SPIO uptake with a significant signal loss in a T2-w FSE sequence in contrast to malignant lesions. When a threshold of 25% is used, PSIL is an accurate tool for the characterization of benign and malignant lesions. For the detection of malignant lesions, the add-on of a CE-T2*-w GRE sequence is helpful due to the significant higher CNR, a superior lesion conspicuity and better image quality in comparison to the CE-T2-w FSE sequence.

With 3D-GRE sequences after bolus-injection of ferucarbotran the differentiation between benign and malignant lesions and the characterization of benign lesions may be

possible. Both 2D- and 3D- GRE techniques do not provide the same information about

liver lesion vascularity as gadolinium-enhanced MRI.

Zusammenfassung

Die Superparamagnetic Iron Oxides (SPIO)-verstärkte MRT der Leber wird als sinnvolle präoperative diagnostische Methode mit einer hohen Sensitivität und Spezifität für die Detektion von fokalen Leberläsionen angewendet. Mit der SPIO-verstärkten MRT ist aber prinzipiell auch eine Differenzierung zwischen benignen und malignen fokalen Leberläsionen möglich auf der Basis ihrer zellulären Zusammensetzung und Funktion (RES-Zellen in normalem Lebergewebe und in benignen Tumoren, keine RES-Zellen in malignen Tumoren).

In früheren Studien wurden die Effekte von SPIO-Kontrastmitteln fast ausschließlich auf die Detektion von Läsionen sowie die Effekte in T2-gewichteten (w) Fast-Spin Echo (FSE) und T2*-w Gradienten Echo (GRE) Sequenzen beschränkt, da SPIO hauptsächlich die T2 / T2* - Zeiten verkürzen.

Ferucarbotran ist ein relativ neu zugelassenes SPIO-Kontrastmittel, welches als intravenöser Bolus appliziert werden kann und sich durch eine geringe Nebenwirkungsrate vor allem im kardiovaskulären Bereich auszeichnet. Eine dynamische T1-w Perfusionsmessung nach der Bolusapplikation von Ferucarbotran könnte Informationen über die Vaskularisation solider Tumore in der Leber liefern. Die Möglichkeit der Charakterisierung von fokalen Leberläsionen mit Hilfe der dynamischen Ferucarbotran-verstärkten MRT wurde bereits in der Literatur angedeutet und typische Befunde konnten an einer begrenzten Anzahl von Fällen für einzelne fokale Leberläsionen gezeigt werden.

Das erste Ziel dieser Arbeit war die Evaluierung der diagnostischen Effizienz des SPIO Kontrastmittel Ferucarbotran in T2-w FSE and T2*-w GRE Sequenzen zur Charakterisierung von fokalen Leberläsionen. Das zweite Ziel war es typische Anreicherungsmuster fokaler Leberläsionen in der dynamischen T1-w MRT mit 2D-GRE and 3D-GRE VIBE Sequenzen zu beschreiben.

An einem 1.5 Tesla MRT-System wurden native und kontrastverstärkte T2-w FSE and T2*-w GRE Sequenzen 10 Minuten nach Bolusinjektion von 1.4 ml Ferucarbotran bei 68 Patienten durchgeführt. An einem 1.5 Tesla MRT-System wurden T1-w dynamische Bilder bei 23 Patienten mit einer 2D-GRE Sequenz und bei 37 Patienten mit einer 3D-GRE-VIBE Sequenz akquiriert.

Die endgültige Diagnose der 68 Patienten, bei denen T2-w FSE/ T2*-w GRE Sequenzen durchgeführt wurden war Hepatozelluläres Karzinom (HCC, n=29), Lebermetastasen (n=15), Cholangiozelluläres Karzinom (CCC, n=2), Hämangiom (n=6), Leberzelladenom (n=5), Fokal Noduläre Hyperplasie (FNH, n=3) und Zysten (n=8). Die endgültige Diagnose der 60 Patienten, bei denen eine T1-w dynamische Ferucarbotran-verstärkte MRT durchgeführt wurde war HCC (n=25), Lebermetastasen (n=14), CCC (n=2), Hämangiom (n=6), Leberzelladenom (n=3), FNH (n=3) and Zysten (n=7). In den T2-w FSE und T2*-w GRE Bildern wurde das Signal-zu-Rausch-Verhältnis (SNR) und das Kontrast-zu-Rausch-Verhältnis basierend auf Signalintensitätsmessungen in den fokalen Läsionen und dem Leberparenchym durchgeführt. Der prozentuale Signalverlust (PSIL) der verschiedenen fokalen Läsionen von der nativen zur

kontrastverstärkten T2-w FSE –Sequenz wurde errechnet. Eine qualitative Auswertung der Bildqualität sowie der Abgrenzbarkeit der Läsionen im Vergleich zwischen kontrastverstärkten T2-w FSE und kontrastverstärkten T2*-w GRE Bildern erfolgte. In den T1-w dynamischen Bildern wurden Signalintensitätsmessungen im Leberparenchym, den Lebergefäßen und in fokalen Leberläsionen vorgenommen um SNR und CNR zu errechnen.

Das mittlere SNR von soliden benignen Läsionen zeigte einen Abfall in der T2-w FSE Sequenz von 34.1 vor auf 21.0 ($p<0,05$) nach Kontrastmittelgabe; maligne Leberläsionen zeigten nur einen geringen Signalverlust von 33.3 auf 32.5 (nicht signifikant). Das mittlere CNR der malignen Läsionen war am höchsten in der kontrastverstärkten T2*-w Sequenz vergleichen mit der nativen- und kontrastverstärkten T2-w FSE Sequenz (29.9 vs. 22.7 ($p<0.01$) vs. 12.8 SI ($p<0.01$)). Bei einem Grenzwert von 25 % Signalverlust (PSIL) in der T2-w FSE Sequenz konnte eine Sensitivität und Spezifität von 97.8% beziehungsweise 92.9% mit der Ferucarbotran-verstärkten T2-w MRT erreicht werden. Der Signalverlust (PSIL) von Adenomen und FNH zeigte keine Überschneidungen. Kontrastverstärkte T2*-w GRE Bilder zeichneten sich durch eine überlegene Bildqualität und Abgrenzbarkeit von Läsionen ($p < .05$) im Vergleich zur kontrastverstärkten T2-w FSE Sequenz aus. In der dynamischen Ferucarbotran-verstärkten T1-w MRT konnte eine Hypervaskularisation in den typischerweise hypervaskularisierten Läsionen wie HCC, Adenom oder FNH nicht gezeigt werden. In Hämangiomen hingegen war ein frühes Enhancement in allen Fällen abzugrenzen. In der T1-w 3D-GRE Sequenz lag das mittlere CNR der soliden benignen Läsionen bei etwa null (FNH) oder war sogar positiv (Adenom), während das mittlere CNR der

malignen Läsionen im negativen Bereich zu allen Zeitpunkten lag.

Zusammenfassend konnte gezeigt werden, dass solide benigne Läsionen eine SPIO-Speicherung zeigen, welche einen signifikanten Signalabfall in den Läsionen in T2-w Bildern hervorruft. Mit einem Grenzwert von 25% Signalverlust (PSIL) kann eine sichere Unterscheidung von benignen und malignen Läsionen erfolgen. Für die Detektion von Läsionen ist eine zusätzliche T2*-w Sequenz hilfreich wegen des stärkeren Läsion-zu-Leber-Kontrastes (CNR), einer verbesserten subjektiven Abgrenzbarkeit der Läsionen und der besseren Bildqualität. Mit der dynamischen T1-w MRT mit einer 3D-GRE Sequenz nach Bolusinjektion von Ferucarbotran können möglicherweise Aspekte zur Charakterisierung von malignen versus benignen Leberläsionen gewonnen werden. Allerdings liefert die T1-w dynamische MRT offensichtlich weder mit 2D- noch mit 3D-GRE Sequenzen die gleiche Information über die Vaskularisation von Leberläsionen wie die Gadolinium-verstärkte MRT, da die von den extrazellulären Kontrastmitteln bekannten Anreicherungsphänomene in hypervaskularisierten Leberläsionen mit der dynamischen Ferucarbotran-verstärkten MRT nicht nachvollzogen werden konnten.

Für die Praxis bedeutet dies, dass der Schwerpunkt der Ferucarbotran-verstärkten MRT Untersuchung weiterhin bei den T2-w und T2*-w Sequenzen liegt, um die in der Literatur berichteten hohen Detektionsraten und die von uns untersuchten Möglichkeiten zur Charakterisierung auszunutzen. Die während der Bolusapplikation durchgeführte T1-w dynamische Bildgebung kann in limitierten Fällen wie z.B. Hämangiomen differentialdiagnostische Hilfestellungen liefern, kann aber die Information einer dynamischen Untersuchung mit extrazellulären Kontrastmitteln nicht ersetzten.

References

1. Arbab AS, Ichikawa T, Araki T, et al. Detection of hepatocellular carcinoma and its metastases with various pulse sequences using superparamagnetic iron oxide (SHU-555-A). Abdom Imaging 2000;25:151-158

2. Bartolozzi C, Lencioni R, Donati F, Cioni D. Abdominal MR: liver and pancreas. Eur Radiol 1999;9:1496-1512

3. Bartolozzi C, Cioni D, Donati F, Lencioni R. Focal liver lesions: MR imaging-pathologic correlation. Eur Radiol 2001;11:1374-1388

4. Ba-Ssalamah A, Heinz-Peer G, Schima W, et al. Detection of focal hepatic lesions: comparison of unenhanced and SHU 555 A-enhanced MR imaging versus biphasic helical CTAP. J Magn Reson Imaging 2000;11:665-672

5. Bellin MF, Zaim S, Auberton E, et al. Liver metastases: safety and efficacy of detection with superparamagnetic iron oxide in MR imaging. Radiology 1994;193:657-663

6. Blakeborough A, Ward J, Wilson D, et al. Hepatic lesions detection at MR imaging: A comparative study with four sequences. Radiology 1997; 203:759-765

7. Bluemke DA, Soyer P, Fishman E. Nontumorous low-attenuation defects in the liver on helical CT during arterial portography: frequency, location, and appearance. AJR 1995;164:1141-1145

8. Castells A, Bruix J, Bru C, at al. Treatment of small hepatocellular carcinoma in cirrhotic patients: a cohort study comparing surgical resection and percutaneous ethanol injection. Hepatology 1993;18:1121-1126

9. Chambon C, Clement O, Blanche RL, Schouman-Claeys E, Frija G. Superparamagnetic iron oxides as positive MR contrast agents: in vitro and in vivo evidence. Magn Reson Imaging 1993;11:509-519

10. Choi D, Kim SH, Lim JH, et al. Preoperative detection of hepatocellular carcinoma: ferumoxides-enhanced MR imaging versus combined helical CT during arterial portography and CT hepatic arteriography. AJR 2001;176:475-482

11. Denys A, Arrive L, Servois V, et al. Hepatic tumors: detection and characterization at 1-T MR imaging enhanced with AMI-25. Radiology 1994;193:665-669

12. Fretz CJ, Elizondo G, Weissleder R, Hahn PF, Stark DD, Ferrucci JT. Superparamagnetic iron oxide-enhanced MR imaging: pulse sequence optimization for detection of liver cancer. Radiology 1989;172:393-397

13. Grangier C, Tourniaire J, Mentha G, et al. Enhancement of liver hemangiomas on T1-weighted MR SE images by superparamagnetic iron oxide particles. J Comput Assist Tomogr 1994;18:888-896

14. Hahn PF, Stark DD, Weissleder R, et al. Clinical application of superparamagnetic iron oxide to MR imaging of tissue perfusion in vascular liver tumors. Radiology 1990;174:361-366

15. Hamm B, Mahfouz AE, Taupitz M, et al. Liver metastases: improved detection with dynamic gadolinium-enhanced MR imaging? Radiology 1997;202:677-682

16. Hamm B, Staks T, Taupitz M. SHU 555A: a new superparamagnetic iron oxide contrast agent for magnetic resonance imaging. Invest Radiol 1994;29:S87-S89

17. Hamm B, Staks T, Taupitz M, et al. Contrast-enhanced MR imaging of liver and spleen: first experience in humans with a new superparamagnetic iron oxide. JMRI 1994;4:659-668

18. Hamm B, Thoeni RF, Gould RG, et al. Focal liver lesions: characterization with nonenhanced and dynamic contrast material-enhanced MR imaging. Radiology 1994;190:417-423

19. Harisinghani MG, Saini S, Weissleder R, et al. Differentiation of liver hemangiomas from metastases and hepatocellular carcinoma at MR imaging enhanced with blood-pool contrast agent code-7227. Radiology 1997;202:687-691

20. Hawighorst H, Schoenberg SO, Knopp MV, Essig M, Mittner P, van Kaick G. Hepatic lesions: morphologic and functional characterization with multiple breath-hold 3D gadolinium-enhanced MR angiography—initial results. Radiology 1999;210:89-96

21. Heiken JP, Weyman PJ, Lee JKT, et al. Detection of focal hepatic masses: prospective evaluation with CT, delayed CT, CT during arterial portography, and MR imaging. Radiology 1989;171:47-51

22. Hughes KS, Simon RM, Songhorabodi S, et al. Resection of the liver for colorectal carcinoma metastases: a multi-institutional study of indications for resection. Registry of hepatic metastases. Surgery 1988;103:278-288

23. Kamel IR, Bluemke DA. MR imaing of liver tumors. Radiol Clin N Am 2003;41:51-65

24. Kanematsu M, Itoh K, Matsuo M, et al. Malignant hepatic tumor detection with ferumoxides-enhanced MR imaging with a 1.5-T system: comparison of four imaging pulse sequences. J Magn Reson Iaging 2001;13:249-257

25. Kopp AF, Laniado M, Dammann F, et al. MR imaging of the liver with Resovist: safety, efficacy, and pharmacodymic properties. Rdiology 1997;204:749-756

26. Langmo LS, Dagher AP, Mehard WB, et al. Does CTAP prior to hepatic resection improve patient survival rates? Abdom Imaging 1994;19:317-319

27. Lee VS, Lavelle MT, Rofsky NM, et al. Hepatic MR imaging with a dynamic contrast-enhanced isotropic volumetric interpolated breath-hold examination: feasibility, reproducibility, and technical quality. Radiology 2000;215:365-372

28. Marchal G, Van Hecke P, Demaerel P, et al. Detection of liver metastases with superparamagnetic iron oxide in 15 patients: results of MR imaging at 1.5 T. AJR 1989;152:771-775

29. Matsui O, Takashima T, Kadoya M, et al. Dynamic computed tomography during arterial portography: the most sensitive examination for small hepatocellular carcinomas. J Comput Assist Tomogr 1985;9:19-24

30. McFarland EG, Mayo SW, Saini S, Hahn PF, Goldberg MA, Lee M. Hepatic hemangiomas and malignant tumors: improved differentiation with heavily T2-weighted conventional spin-echo MR imaging. Radiology 1994;193:43-47

31. McNicholas M, Saini S, Echeverri J, Foley M, Kaufman J, McFarland E. T2 relaxation times of hypervascular and non-hypervascular liver lesions: do hypervascular lesions mimic hemangiomas on heavily T2-weighted MR images? Clin Radiol 1996;51:401-405

32. Mergo PJ, Helmberger T, Nicolas AI, Ros PR. Ring enhancement in ultrasmall superparamagnetic iron oxide MR imaging: a potential new sign for characterization of liver lesions. AJR 1996;166:379-384

33. Mintorovitch J, Shamsi K. Eovist injection and Resovist injection: two new liver-specific contrast agents for MRI. Oncology 2000;14:37-40

34. Müller M, Reimer P, Wiedermann D, et al. T1-weighted dynamic MRI with new superparamagnetic iron oxide particles (Resovist): results of a phantom study as well as 25 patients. Rofo Fortschr Geb Roentgenstr Neuen Bildgeb Verfahr 1998;168:228-236

35. Oudkerk M, Van den Heuvel AG, Wielopolski PA, Schmitz PIM, Borel Rinkes IHM, Wiggers T. Hepatic lesions: detection with ferumoxide-enhanced T1-weighted MR imaging. Radiology 1997;203:449-456

36. Paley MR, Mergo PJ, Torres GM, Ros PR. Characterization of focal hepatic lesions with ferumoxides-enhanced T2-weighted MR imaging. AJR 2000;175:159-163

37. Pawluk RS, Tummala S, Brown JJ, Borrello JA. A retrospective analysis of the accuracy of T2-weighted images and dynamic gadolinium-enhanced sequences in the detection and characterization of focal hepatic lesions. JMRI 1999;9:266-273

38. Peterson MS, Baron RL, Dodd GD, et al. Hepatic parenchymal perfusion defects detected with CTAP: imaging-pathologic correlation. Radiology 1992;185:149-155

39. Reimer P, Müller M, Marx Christian, et al. T1 effect of a bolus-injectable superparamagnetic iron oxide, SHU 555 A: dependence on field strength and plasma concentration- preliminary clinical experience with dynamic T1-weighted MR imaging. Radiology 1998;209:831-836

40. Reimer P, Rummeny EJ, Daldrup HE, et al. Clinical results with Resovist: a phase 2 clinical trial. Radiology 1995;195:489-496

41. Reimer P, Tombach B. Hepatic MRI with SPIO: detection and characterization of focal liver lesions. Eur Radiol 1998;8:1198-1204

42. Rofsky NM, Lee VS, Laub G, et al. Abdominal MR imaging with a volumetric interpolated breath-hold examination. Radiology. 1999;212:876-884

43. Ros PR, Freeny PC, Harms SE, et al. Hepatic MR imaging with ferumoxides : a multicenter clinical trial of the safety and efficacy in the detection of focal hepatic lesions. Radiology 1995;196:481-488

44. Saini S, Edelman RR, Sharma P, et al. Blood-pool MR contrast material for detection and characterization of focal hepatic lesions: initial clinical experience with ultrasmall superparamagnetic iron oxide (AMI-227). AJR 1995;164:1147-1152

45. Seltzer SE, Holman BL. Imaging of hepatic metastases from colorectal carcinoma: identification of candidates for partial hepatectomy. Radiology 1989;152:917-923

46. Semelka RC, Schlund JF, Molina PL, et al. Malignant liver lesions: comparison of spiral CT arterial portography and MR imaging for diagnostic accuracy, cost, and effect on patient management. JMRI 1996;1:39-43

47. Semelka RC, Worawattanakul S, Kelekes NL, et al. Liver lesion detection, characterization, and effect on patient management: comparison of single-phase spiral CT and current MR techniques. JMRI 1997;7:1040-1047

48. Senéterre E, Taourel P, Bouvier Y, et al. Detection of hepatic metastases: ferumoxides-enhanced MR imaging versus unenhanced MR imaging and CT during arterial portography. Radiology 1996;200:785-792

49. Small WC, Nelson RC, Bernardino ME. Dual contrast enhancement of both T1- and T2-weighted sequences using ultrasmall superparamagnetic iron oxide. Magn Reson Imaging 1993;11:645-654

50. Soyer P, Levesque M, Caudron, A, Elias E, Zeitoun G, Roche A. MRI of liver metastases from colorectal cancer vs. CT during arterial portography. J Comput Assist Tomogr 1993;17:67-74

51. Tang Y, Yamashita Y, Arakawa A, et al. Detection of hepatocellular carcinoma arising in cirrhotic livers: comparison of gadolinium- and ferumoxides-enhanced MR imaging. AJR 1999;172:1547-1554

52. Uchida H, Matsuo N, Sakaguchi H, Nagano N, Nishimine K, Ohishi H. Segmental embolotherapy for hepatic cancer: keys to success. Cardiovasc Intervent Radiol 1993;16:67-71

53. Van Beers BE, Lacrosse M, Jamart J, et al. Detection and segmental location of malignant hepatic tumors: comparison of ferumoxides-enhanced gradient-echo and T2-weighted spin-echo MR imaging. AJR 1997;168:713-717

54. Vogl TJ, Hammerstingl R, Schwarz W, et al. Magnetic resonance imaging of focal liver lesions: comparison of the superparamagnetic iron oxide Resovist versus gadolinium-DTPA in the same patient. Invest Radiol 1996;31:696-708

55. Vogl TJ, Hammerstingl R, Schwarz W, et al. Superparamagnetic Iron Oxide-enhanced versus Gadolinium-enhanced MR imaging for differential diagnosis of focal liver lesions. Radiology 1996;198:881-887

56. Wang YJ, Hussain SM, Krestin GP. Superparamagnetic iron oxide contrast agents: physicochemical characteristics and applications in MR imaging. Eur Radiol 2001;11:2319-2331

57. Yamada R, Sato M, Kawabata M, Nakatsuka H, Nakamura K, Takashima, S. Hepatic arterial embolization in 120 patients with unresectable hepatoma. Radiology 1983;148:397-401

58. Yamamoto H, Yamashita Y, Yoshimatsu S, et al. Hepatocellular carcinoma in cirrhotic livers: detection with unenhanced and iron oxide-enhanced MR imaging. Radiology 1995;195:106-112

59. Yamashita Y, Hatanaka Y, Yamamoto H, et al. Differential diagnosis of focal liver lesions: role of spin-echo and contrast-enhanced dynamic MR imaging. Radiology 1994;193:59-65

List of Publications

a. <u>Namkung S</u>, Zech CJ, Helmberger T, Reiser MF, Schoenberg SO. Efficacy of Ferucarbotran-enhanced early dynamic MR imaging with T1-weighted sequences for characterization of focal liver lesions. British J Radiology (2006 submitted)

b. <u>Namkung S</u>, Zech CJ, Helmberger T, Reiser MF, Schoenberg SO. Superparamagnetic Iron Oxide (SPIO)-enhanced liver MR imaging with Ferucarbotran: efficacy for characterization of focal liver lesions with T2-weighted FSE and T2*-weighted GRE images. JMRI (June-2006 accepted)

Index of Tables

Index of Graphs

Index of Figures

Acknowledgment

I thank my parents and family for giving me great encouragement with their constant and clement support while I stayed in Munich.

I would like to thank my supervisors Prof. Dr. med. Dr. h.c. M. Reiser and PD Dr. S. Schönberg for help and support during planning and accomplishment of the study.

Finally, special thanks to Dr. C. Zech for sincere help in many situations and guiding me through the data analysis and writing process of this manuscript.

Curriculum Vitae

Personal Data : Sook Namkung
  Birth Date : 17.04.1966
  Birth Place : Chuncheon, South Korea
  Parents : Hyeon Namkung
    : Jeong-Yeo Heo

School Education :
  1972 – 78 : Bongeuy Elementary School, Chuncheon, South Korea
  1978 – 81 : Bongeuy Girls Middle School, Chuncheon, South Korea
  1981 – 84 : Yoobong Girls High School, Chuncheon, South Korea

Academic Education and Appoinments :
  1984 – 90 : College of Medicine, Hallym University, Chuncheon, South Korea (Doctor of Medicine)
  9/96 – 8/98 : Graduate School, Hallym University, Chuncheon, South Korea (Diagnostic Radiology, Master's Degree of Medical Science)
  1990 – 91 : Internship, Kangdong Sacred Heart Hospital, Hallym University, Seoul, South Korea
  1991 – 95 : Residentship, Kangdong Sacred Heart Hospital, Hallym University, Dept. of Diagnostic Radiology, Seoul, South Korea
  1995 – 96 : Fellowship, Samsung Medical Center, Sungkyunkwan University, Dept. of Diagnostic Radiology, Seoul, South Korea
  1996 – 2000 : Instructor, Diagnostic Radiology, College of Medicine, Hallym University, Chuncheon, South Korea
  2000 – : Assistant Professor, Diagnostic Radiology, College of Medicine, Hallym University, Chuncheon, South Korea